รายงานวิจัยฉบับสมบูรณ์

โครงการ
ชุดสมการสำหรับวิเคราะห์และคำนวนตัวแปรสำคัญของคลื่นน้ำบนพื้นฐานของสเปกตรัมพลังงานคลื่นผิวน้ำ

(Analytical Solutions for Estimating Phase-Averaged Water Wave Parameters based on Surface Wave Energy Spectra)

โดย

ผศ.ดร.ชัชวิน ศรีสุวรรณ

(Assistant Professor Dr. Chatchawin Srisuwan)

มิถุนายน 2560

(JUNE 2017)

สัญญาเลขที่ TRG5880184

รายงานวิจัยฉบับสมบูรณ์

โครงการ
ชุดสมการสำหรับวิเคราะห์และคำนวนตัวแปรสำคัญของคลื่นน้ำบนพื้นฐานของสเปกตรัมพลังงานคลื่นผิวน้ำ
(Analytical Solutions for Estimating Phase-Averaged Water Wave Parameters based on Surface Wave Energy Spectra)

ผศ.ดร.ชัชวิน ศรีสุวรรณ
ภาควิชาวิศวกรรมโยธา คณะวิศวกรรมศาสตร์
มหาวิทยาลัยสงขลานครินทร์

สนับสนุนโดยสำนักงานกองทุนสนับสนุนการวิจัยและ
มหาวิทยาลัยสงขลานครินทร์

รหัสโครงการ: TRG5880184

ชื่อโครงการ: ชุดสมการสำหรับวิเคราะห์และคำนวนตัวแปรสำคัญของคลื่นน้ำบนพื้นฐานของสเปกตรัมพลังงานคลื่นผิวน้ำ

ชื่อนักวิจัย: ผศ.ดร.ชัชวิน ศรีสุวรรณ ภาควิชาวิศวกรรมโยธา คณะวิศวกรรมศาสตร์ มหาวิทยาลัยสงขลานครินทร์

E-mail Address : chatchawin.s@psu.ac.th

ระยะเวลาโครงการ: 24 เดือน (กรกฎาคม 2558 - มิถุนายน 2560)

บทคัดย่อ

ค่าเฉลี่ยของตัวแปรคลื่นต่างๆ อาทิเช่น การเคลื่อนตัวของโมเมนตัม มวลน้ำ และพลังงานคลื่น มีความสำคัญเป็นอย่างยิ่งต่อการศึกษาคลื่นผิวน้ำรวมถึงการจำลองกระบวนการหมุนวนในมหาสมุทร งานวิจัยชิ้นนี้จัดทำขึ้นเพื่อคิดค้นและพัฒนาสูตรใหม่สำหรับการคำนวนค่าตัวแปรของคลื่นดังกล่าว การศึกษาวิจัยประกอบด้วยสองส่วนหลักคืองานศึกษาด้านทฤษฎีและงานสำรวจและรวบรวมข้อมูลการตรวจวัดคลื่นจริงในภาคสนาม การคิดค้นสูตรคำนวนได้บรรลุโดยการใช้สมการเทียบเคียงและใช้สเปกตรัมสังเคราะห์เป็นตัวแทนสเปกตรัมพลังงานคลื่น สูตรการคำนวณใหม่ที่คิดค้นได้อยู่ในรูปของสูตรสำเร็จที่พร้อมใช้งานโดยคำนึงถึงอิทธิพลจากคลื่นแบบสุ่มขนาดต่างๆทั้งหมดที่อาจมีอยู่ในท้องทะเล ณ ขณะหนึ่ง การพิสูจน์โดยใช้ค่าคลื่นสังเคราะห์แสดงให้เห็นว่าสมการใหม่ที่ได้สามารถใช้ได้ดีกับสเปกตรัมคลื่นในระดับน้ำลึกปานกลางถึงระดับความลึกสูง การวิเคราะห์ความอ่อนไหวยืนยันว่าสมการดังกล่าวสามารถใช้งานได้ดีในสภาวะคลื่นในช่วงความรุนแรงปกติซึ่งเป็นสภาวะส่วนใหญ่ในท้องทะเล ในการพิสูจน์ความแม่นยำค่าตัวแปรที่คำนวนได้จากสมการใหม่ได้ถูกเปรียบเทียบกับค่าตัวแปรที่ได้จากสเปกตรัมคลื่นจากการตรวจวัดภาคสนาม ผลการเปรียบเทียบแสดงให้เห็นว่าสูตรใหม่ที่คิดค้นขึ้นในงานวิจัยนี้ซึ่งคำนึงถึงคลื่นแบบสุ่มทั้งหมดสามารถเพิ่มความแม่นยำในการคำนวณผลลัพท์กว่า 5-10% เมื่อเทียบกับวิธีการเดิมที่ใช้อยู่ทั่วไปซึ่งทำการคำนวนค่าผลลัพท์โดยอ้างอิงค่าตัวแปรหลักจากคลื่นตัวแทนเท่านั้น

คำหลัก: คลื่นผิวน้ำ, ค่าตัวแปรคลื่นเฉลี่ย, ค่าสเปกตรัมพลังงานคลื่น, ค่าสเปกตรัมพลังงานคลื่นสังเคราะห์

Project Code : TRG5880184

Project Title : Analytical solutions for estimating phase-averaged water wave parameters based on surface wave energy spectra

Investigator : Assistant Professor Dr. Chatchawin Srisuwan, Department of Civil Engineering, Faculty of Engineering, Prince of Songkla University

E-mail Address : chatchawin.s@psu.ac.th

Project Period : 24 Months (JULY 2015 - JUNE2017)

Abstract

Phase-averaged quantities such as radiation stress, energy flux, and mass flux are essential parameters in the study of surface water waves and in the modeling of ocean circulation. This research project aims at developing a novel set of formulas for estimating these dynamic wave parameters. The study was accomplished via two parts: the theoretical desk study and the field data collection. The latter task involved launching an in-situ measurement platform and assimilation of other available wave data. The theoretical development was achieved based on asymptotic analysis on linear wave theory with aids of parameterized wave spectra. The new formulas obtained are in closed forms and ready for analytical application while considering the contribution from the entire random wave field. Verification against synthetic wave data reveals that the formulas are best suitable in transitional to deep water condition. Sensitivities of the formulas were analyzed via an aid of reliable field wave spectra and no concern for their application was found in any regular sea states. The new analytical formulas were also validated against nine collections of field wave spectra. The final validation confirms that, in terms of both accuracy and precision, the formulas could offer about 5 - 10 % improvement over the traditional representative wave approach which allows an estimation based solely on some nominal waves.

Keywords : surface water waves, phase-averaged wave parameters, wave energy spectra, parameterized wave spectra.

Contents

List of Figures and Tables

Figures

Table

1 Introduction

Complex wave fields in the coastal ocean are often described by a group of phase-averaged wave parameters including basic wave heights and periods and other derived terms such as wave energy, wave energy flux, wave mass flux, and wave radiation stress. These parameters are all important for use in the simulation of physical processes in the sea and are almost always required as inputs in the engineering design. The radiation stress and its concept introduced by Longuet-Higgins and Stewart (1964) permits modeling of time-averaged, wave-driven circulation in the nearshore zone that can be incorporated as part of sediment transport and morphology models.

As per the existing practice, two common means of estimating phase-averaged wave parameters are applied. One is to perform the estimation by numerically integrating a full wave spectrum, measured or parametrized, in order to account for all random waves with different frequencies and their contribution to the wave parameter of interest. The other common method is to predict the parameter based on a single representative wave. In this latter case, it is assumed that the wave field is narrow-banded and the target parameter could be predicted based on the most significant parameters such as the significant wave height $H_{1/3}$ and the associated wave period $T_{1/3}$.

In the present study, two novel formulas were derived and introduced for the estimation of the wave radiation stresses and the wave mass flux. While appearing in closed forms and ready for analytical application, the new formulas were proved to offer enhanced estimation accuracies, surpassing those allowed by the representative wave approach. The literature review of the problem starts in the next section, followed by the outline of proposal on this research work.

The collections of wave data which were utilized in testing the formulas are subsequently explained. The derivation of the formulas was later described and evaluation and verification of the new solutions are shown, including a sensitivity test on the formulas to ensure their applicable ranges. Conclusions of the study are finally made to summarize the underlying bases and practical utilities of the new formulas.

2 Literature Review

2.1 Background and Relevant Study

Momentum and mass balance of fluid over a train of water waves is typically described in terms of wave radiation stress and wave mass flux. These important wave parameters allow the explanation for many essential phenomena in the sea, including wave setup and set down, undertow, longshore current, edge waves, and shear waves (e.g. Svendsen 2006; Davidson-Arnott 2010). An effective means to determine the parameters is thus required in a wide range of water depths. The accuracy in the determination often features a direct impact on the preparation of wave climatology data (e.g. Hughes 2004; Wargula et al. 2013). As a consequence, the capability in the estimation of the wave radiation stress and wave mass flux may become very crucial to the performance of both ocean circulation and coastal morphodynamic models (e.g. De Vriend and Stive 1987; Haas et al. 2003; Srisuwan and Work 2015).

In a phase-averaged sense, the radiation stress and wave mass flux are estimated per their total quantities over the wave period. Some advanced wave theory permits the estimation on a phase-resolving, wave-by-wave basis (e.g. Rakha 1998; Li et al. 2007). The intra-wave approach may enable a direct simulation of non-linear wave phenomena, but sometimes dynamic processes that involve uncertainty and randomness still could not be described clear enough for implementing such a fully wave-resolving scheme. The use of the phase-averaged estimation, meanwhile, has been attempted in many research efforts to show that such an approach could lead to satisfactory modeling results under a wide range of wave conditions (e.g. Ding et al. 2006; Haas and Warner 2009; Cambazoglu and Haas 2011).

For monochromatic sinusoidal waves, the airy wave theory may be applied for an estimation of the wave mass flux and wave radiation stress following the original concept suggested by Longuet-Higgins and Stewart (1964). In a random wave field, two typical means for the estimation are found in current practice (e.g. Dean and Dalrymple 1991; Holthuijsen 2007). A numerical integration may be performed on a full surface wave energy spectrum obtained via measurement or parametrization. This method will account for incremental contributions from all individual waves considering their frequency-dependent magnitudes and kinematics. The other simpler means to approximate the parameters is often referred to as a representative wave approach in which the estimation of the parameters is based solely on some nominal waves under an ideal assumption of a narrow-banded wave field.

Improvements in the estimation of the wave radiation stress and the wave mass flux are found in the literature, most of which are achieved by use of extended wave theory for describing the wave quantities and their variations. Stive and Wind (1982) applied two nonlinear wave theory and showed that they both are superior to the linear theory in the determination of the radiation stress and wave setup. Wang et al. (2008) introduced new expressions of the wave radiation stress and volume flux reformulated by including up to the sixth-order description of surface waves. The new formulas were incorporated in a circulation model to show a more accurate estimation for wave setup and setdown in the domain with, however, a very marginal effect on the vertical profile of wave-induced currents.

More practical improvements on the subject area have been focused on estimating the parameters for a group of random waves, motivated by the fact that a narrow-band representation of the waves may cause the resulting parameters to deviate significantly from their actual quantities in the sea (Tayfun, 1986). In this type of study, the parameters obtained via a full numerical integration on the random wave spectra are typically treated as the factual best estimates for comparison purpose. Feddersen (2004) attempted to analyze various sets of measured wave data before revealed that the narrow-banded approximation could lead to around 35% overestimation in the radiation stress. The selection of waves to serve for the representative parameters alone could lead to much inconsistency in the estimation.

2.2 Basic Theory

In this section, fundamental principles in quantifying and expressing basic wave parameters are described which lead to the estimation of important phase-averaged wave parameters. According to linear wave theory, any wave parameters recorded at a measurement point will feature contribution from waves with many different frequencies, described in the form of a periodic Fourier series as

$$F(x,y,z,t) = \frac{A_o}{2} + \sum_{n=0}^{N} \left[A_n \cos(n\omega t) + B_n \sin(n\omega t)\right] \tag{2.1}$$

where ω is the angular wave frequency; N is the total number of wave frequencies considered; A_o, A_n and B_n are the Fourier coefficients that depend on the wave parameter of interest. If the discrete values in this time series are transformed into a frequency domain, a

spectrum of the wave parameter can be created. For example, a time series of water surface displacements $\eta(t)$ may be processed to yield a non-directional wave energy spectrum $S_\eta(f)$ of the wave field that follows

$$S_\eta(f) = \frac{(A_n^2 + B_n^2)}{2\Delta\omega} \tag{2.2}$$

in which f indicates the wave frequency. If wave directions are also considered, a directional spreading function $D(f, \alpha)$ can be multiplied to this wave spectrum to represent a directional wave energy spectrum

$$E(f, \alpha) = S_\eta(f)\, D(f, \alpha) \tag{2.3}$$

in which the wave direction is denoted by α. Since the total wave energy must be conserved, the directional spreading function must follow the constraint $\int_0^{2\pi} D(f, \alpha)\, d\alpha = 1$. Once Equation (2.3) is integrated over all possible directions, the result therefore will be the non-directional energy spectrum $S_\eta(f)$ in Equation (2.2).

Although a wave measurement scheme would allow accurate estimates of $S_\eta(f)$, such an in-situ technique is very limited considering amounts of cost and time required, as well as the immense extent of the coastal ocean. An alternative has been proposed to represent the wave spectrum via parameterization. For example, Pierson and Moskowitz (1964) suggested that a fully-developed surface waves in deep water should feature the distribution of the wave energy following the form

$$S_\eta^{PM}(f) = \vartheta g^2 (2\pi)^{-4} f^{-5} \exp\left[-\frac{5}{4}\left(\frac{f}{f_p}\right)^{-4}\right] \tag{2.4}$$

where f_p is the peak wave frequency, and ϑ is an empirical coefficient. Later, two major improvements of this parameterized wave spectrum were performed. One was to account for the fetch and duration limits of wave generation, leading to the so-called JONSWAP wave spectrum (Hasselman et al., 1973). The other modification was proposed to account for effect of finite water depth on the wave field (Bouws et al., 1985), resulting in what is known to day as the TMA wave spectrum

$$S_\eta^{TMA}(f) = S_\eta^{PM}\, \gamma^\delta\, \phi_k \tag{2.5}$$

in which γ^{δ} is the peak enhancement factor that makes it a JONSWAP spectrum, and ϕ_k is the water depth dependency factor in the TMA spectrum, given as

$$\phi_k(f,h) = \frac{\left[k(f,h)^{-3}\dfrac{\partial k(f,h)}{\partial f}\right]}{\left[k(f,\infty)^{-3}\dfrac{\partial k(f,\infty)}{\partial f}\right]} \tag{2.6}$$

where h and k are the water depth and the wave number, respectively.

By use of linear wave theory, spectral estimates of important wave parameters can be determined based on the surface wave energy spectrum. For example, wave radiation stresses, S_{xx} and S_{xy}, can be described based on the components in all possible wave directions and frequencies following

$$S_{xx} = \int_0^{\infty}\int_0^{2\pi} E(f,\alpha)\left[\frac{C_g(f)}{C(f)}\sin(\alpha)\cos(\alpha)\right]\, d\alpha\, df \tag{2.7}$$

$$S_{xy} = \int_0^{\infty}\int_0^{2\pi} E(f,\alpha)\left[\frac{C_g(f)}{C(f)}(\cos^2(\alpha)+1)-\frac{1}{2}\right]\, d\alpha\, df \tag{2.8}$$

in which C and C_g are the frequency-dependent celerity and group celerity of the waves, respectively. Note that equations of similar forms can be expressed for other wave parameters such as wave energy, wave energy flux, and wave mass flux. In the present body of knowledge, numerical integration of such equations is the only means to estimate the wave parameters in this scenario.

3 Proposed Study

The main idea in this research work is to develop a new analytical tool for estimation of phase-averaged wave parameters, thus eliminating the complex needs in the wave spectral simulation and modification, as well as the numerical computation procedure. The goals in this research work were set and accomplished under the following outlines.

3.1 Objectives

To obtain a set of novel analytical solutions that serve as an accurate predictive tool for phase-averaged wave parameters, the following objectives were set:

1. To mathematically develop new analytical solutions for estimation of wave parameters;
2. To test the new formulas against available numerical solutions for prediction accuracy;
3. To obtain field wave data via a measurement scheme and from database available worldwide;
4. To evaluate and validate the new analytical formulas with the field data;
5. To illustrate advancement that the new formulas offer in engineering applications.

3.2 Scope of Study

Given the ultimate goal to expand the body of knowledge in the analysis of phase-averaged wave parameters, this research work was separated into two phases: theoretical desk study and field investigation. These two tasks were later interpreted together in the final, but each consisted of different scopes.

- The desk study was focused on finding new solutions for at least three important wave parameters. Parameterized wave spectra were first employed, and modified as appropriate, in order to approach the solutions. A wide range of mathematical functions and tools were utilized in the study together with the mechanics of linear wave theory. Some approximation or truncation of terms in original expressions became to be necessary in the solution methods.

- The field work effort was made and data sets of waves were collected for a long period of time at some different sites which feature intermediate water depths. The raw data were wave-induced pressures that could be processed for wave energy spectra, from which the spectral estimates of target wave parameters could be obtained. Acquisition of the data sets were designed such that various wave conditions were captured. Each set of the wave records could represent the wave conditions and their variations over a period of 24 hours.

Finally, capability of the new solutions developed in this study were evaluated by comparing their results with corresponding spectral estimates obtained from field wave spectra. Note that the evaluation was not only subject to the self-measured sets of data, but also performed based on other data sets available worldwide.

A couple of indicators were constrained in the evaluation. First, the results reproduced from the new solutions must be closer to the spectral estimates than possible results determined under the representative single wave assumption. The other, more ambitious indicator could be justified if the new solutions yield target results that are different from

the spectral estimates within the measurement uncertainty. This latter vindication implies that a better test for the solutions would not even be sensible given the present state of the art in surface wave measurement.

3.3 Expected Benefits

Upon the success, this research work is believed to contribute to a new body of knowledge in surface wave analysis in coastal and ocean engineering, with the following outputs:

- New formulas for estimation of phase-averaged wave parameters;
- New data sets of surface wave energy spectra measured in Thailand;
- New assembled sets of spectral wave data in the nearshore zone;
- Article published in a prestigious journal providing guideline for use of the new method and direction for future related research.

The contribution may be perceived as a major step forward in the subject area since practical applications of the above outputs can include:

- Incorporation of the new formulas in numerical morphodynamic modeling systems to
  - increase accuracy and reduce computational demand,
  - help reduce the need for complex surface wave measurement scheme,
  - allow modeling of cases without available full spectral wave information,
- Use of field data sets as part of regional wave climate database to
  - encourage theoretical analysis based on the data,
  - allow use as numerical modeling inputs.

4 Acquisition of Wave Data

Beside the theoretical desk study, another major task in this research project was the preparation of wave data for validating and verifying the newly developed formulas. This task included launching a few measurement campaigns for collecting regional field wave data, as well as gathering measured wave data which were already available worldwide. The processes through which the target sets of data could be obtained are delineated below.

4.1 Design and Fabrication of Measurement Platform

A complete design and fabrication of a wave measurement platform is first shown here since it was an important unit required as part of the field data collection campaigns. The first few criteria for the design laid in the facts that the fabricated frame must be able to 1) hold the proposed sensors in the desired positions, 2) withstand harsh waves and currents in the sea , and 3) allow reasonable convenience for assembling, transportation, deployment, and retrieval in the actual application.

The platform was designed to be a stainless steel frame consisting of multiple assembles. The basement of the frame is shown in Figure 4.1. Four vertical rods with sensors on the tips are to be attached to the basement (Figure 4.2). The main aims in this design are to meet the requirement of practicality in transporting and deploying the unit, as well as to promote its stability once located on the seafloor.

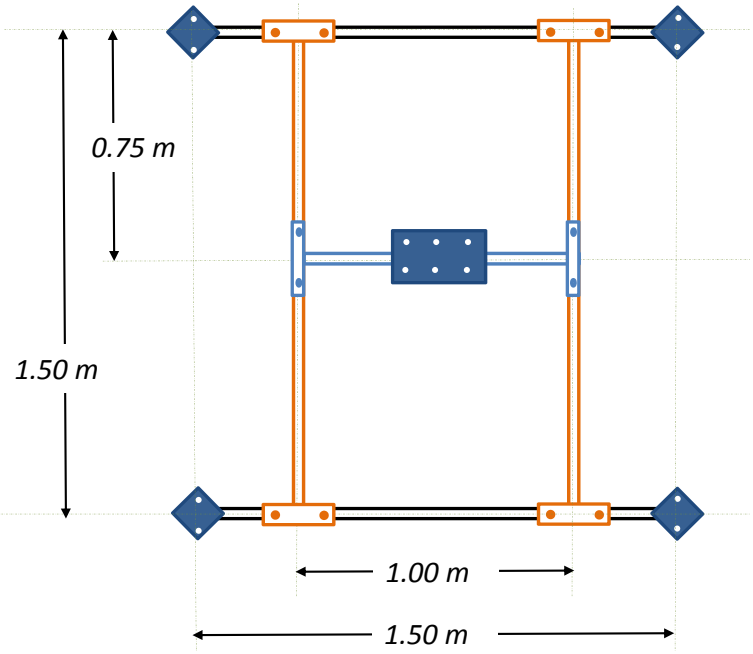

Figure 4.1: Plan view of the measurement platform.

Detailed designs of the assembles that are parts of the basement are shown in Figure 4.3. Between any pair of them, two adjoining spots are used to minimize possible swaying and tilting of the frame. Standard M10 nuts and bolts are used to tighten the parts together. Each of the four vertical rods is attached to the basement and another is used to hold the

sensor as shown in Figure 4.3. The other is then inserted between the upper and the lower parts. Two pieces of this middle arm could be used if a higher elevation of the sensor is needed.

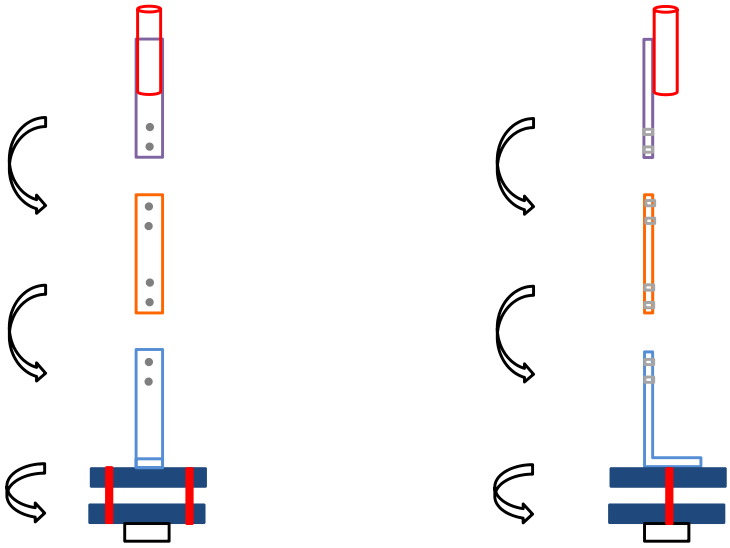

Figure 4.2: Side views of the measurement platform.

Dimensions of each piece of the rod assembles are shown in Figure 4.4. The platform was completed and was initially tested in the field. Figure 4.6 and Figure 4.7 show an on-site assemble of the frame and a shipboard deployment in the preliminary test. The sensors attached to the platform were Solinst pressure loggers (Figure 4.5) which records absolute pressure, including hydrostatic and wave induced portions, at a maximum rate of 8 Hz. Data acquired from the preliminary test were processed to ensure that the utilization of this setup provides sensible results based on the measured data.

4.2 Data Collection and Analysis

The test against field wave data was set as a major focus for demonstrating practical application of the new formulas. With this reason, several field measurement efforts were attempted in the coastal ocean of Thailand.

Before illustrating and discussing about the measurement campaigns, it is worth reviewing basic theory applied in the collection and analysis of wave data. For a measurement of directional wave spectra at a specific location, an array of pressure sensors

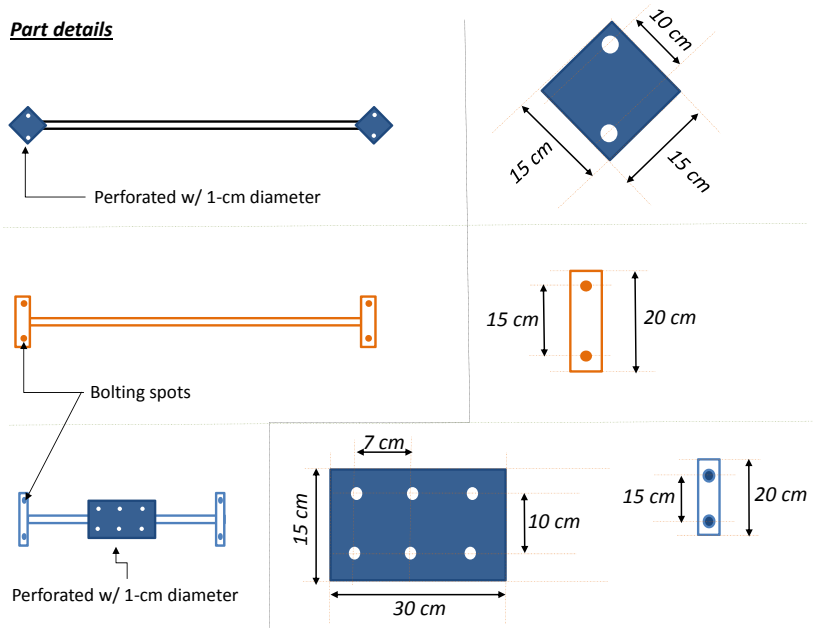

Figure 4.3: Assemble parts of the base structure.

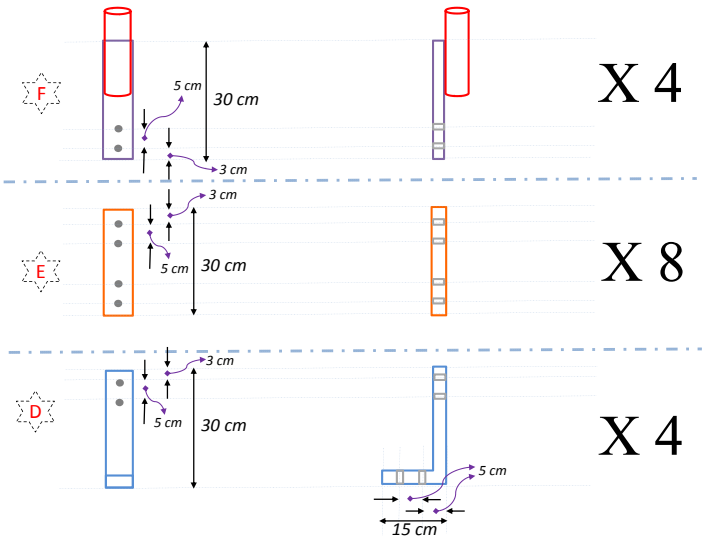

Figure 4.4: Assemble parts of the measurement arms.

Figure 4.5: Solinst pressure sensors equipped with the frame for logging data.

Figure 4.6: Preparation of the measurement frame for deployment.

Figure 4.7: Deployment of measurement platform

need to be deployed for data acquisition. The array must consist of three sensors. In the scenario with the measurement platform here, four pressure sensors were utilized and aligned as shown in Figure 4.8. Each sensor was set to continuously record absolute pressure under the wave field which, for a monochromatic wave, will be appearing to an observer as

$$P(t) = \frac{\rho g H}{2}\left[\frac{\cosh k(h+z)}{\cosh kh}\right]\exp\{i[(k\cos\alpha)x + (k\sin\alpha)y - \omega t]\} \tag{4.1}$$

where α is the wave direction with respect to shore normal. For random waves, all of this record at the four sensors can be converted into surface wave energy spectra $S_\eta(f)$ using a fast Fourier transform algorithm based on the relation

$$P_l(x_p, y_q, t) = \sum_{m=0}^{M}\sum_{n=0}^{N}\left[a_{nm}\cos(\Psi_{nm} + \omega_n t) + b_{nm}\sin(\Psi_{nm} + \omega_n t)\right]\left[\frac{\cosh k_n(h+z)}{\cosh k_n h}\right] \tag{4.2}$$

in which l indicates the device number with corresponding location x_p and y_q; while wave frequency and direction are denoted by n and m respectively. The factor Ψ_{nm} represents the phase function $[(k_n\cos\alpha_m)x_p + (k_n\sin\alpha_m)y_q - \omega t]$.

Four available $S_\eta(f)$ from the four sensors can be utilized as redundant information in the wave spectral analysis, as well as for determining directional spreading of the wave field. The maximum likelihood method by Capon (1969), with improvement by Pawka (1983), may be used for the purpose. Under this technique, a cross spectrum between any pair

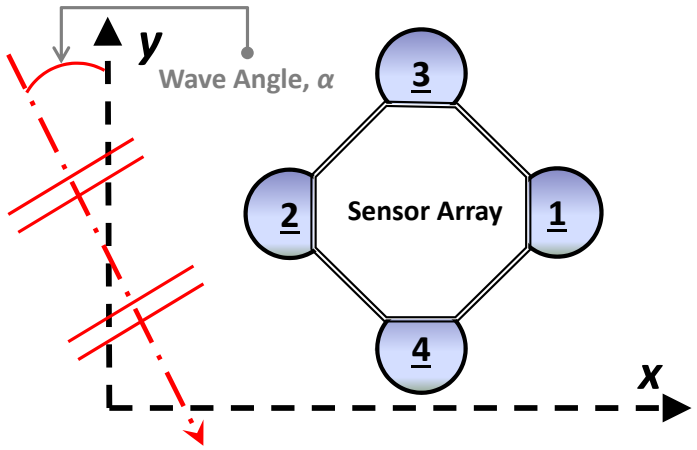

Figure 4.8: Schematic of pressure sensor array for collecting spectral wave data.

of pressure time series can be expressed in terms of wave energy spectrum and associated transfer functions following

$$S_{p,q}(f) = S_\eta(f) \int_0^{2\pi} D(f,\alpha) H_p(f,\alpha) H_q^*(f,\alpha)\, d\alpha \tag{4.3}$$

in which the subscripts p and q indicate pressure sensor numbers 1-4, and the asterisk indicates a complex-transposed function, or the Hermitian conjugate of the original function. The key concept of this method is to determine the directional spreading $D(f,\alpha)$ that has the greatest likelihood of conforming to Equation (4.3). The task is performed by use of an inverse problem that allows

$$D(f,\alpha) = \frac{\Gamma(f)}{\sum_p \sum_q S_{pq}^{-1}(f) H_p(f,\alpha) H_q^*(f,\alpha)} \tag{4.4}$$

where $\Gamma(f)$ is a normalization parameter applied such that the energy is conserved.

The measurement platform and analyzing technique above were adopted in the field data collection efforts at three different locations in the coastal zone of Thailand, including (see also Table 4.1 for details)

1. Pakmeng Bay, Sikao district, Trang province (Andaman Sea);
2. Tambon Tabon, Ranode district, Songkhla province (Gulf of Thailand);

3. Tambon Rawa, Ranode district, Songkhla province (Gulf of Thailand);

4. Thepha Bay, Thepha district, Songkhla province (Gulf of Thailand).

For the first location at Pakmeng Bay, the full application of the platform with four sensors were applied to obtain a total of 259 directional wave spectra. Some examples of the results were shown in Figures 4.9 to 4.11 in which components of wave energy in different frequencies are shown in the top, and their propagation directions are illustrated in the bottom. In all cases, it can be seen that the major portion of wave energy was in the frequency band of 0.05-0.15 Hz which corresponds to the wave periods of 6 to 20 seconds. These wave periods seems rather long but are still in the range of wind-induced surface waves. Meanwhile, the dominating propagation directions were around 250^o-360^o which imply that the wave were propagating towards the shoreline. Note that the 0^o axis was pointed to the north and the angle was defined counterclockwise.

Table 4.1: Details of field measurement campaigns carried out to collected wave data.

No.	**Date**	**Site Details**			
		Location	Approx. Position	$\bar{h}$ (m)	No. of wave spectra
1.	11/20/15 to 12/2/15	Pakmeng	7.507N, 99.308E	2.8	259*
2.	2/1/16 to 2/2/16	Tabon	7.846N, 100.368E	4.3	29
3.		Rawa	7.708N, 100.407E	3.0	28
4.	3/10/16 to 3/16/16	Thepha(1)	6.882N, 101.000E	4.2	166
5.		Thepha(2)	6.887N, 101.014E	5.3	149

For the second and the third locations at Tambon Tabon and Tambon Rawa, only two pressures were deployed at each site to obtain non-directional wave spectra. This alteration was applied since the concurring development of the new analytical formulas indicated that only wave-frequency spectra would be sufficient for the proposed verification and validation. Plus, it has to be admitted that the measurement of directional wave spectra was not as straightforward as outlined. There were too many factors that could possibly affect the precision and accuracy of the measurement results. For example, the synchronization of the data loggers could not be made perfect and possible oscillation of the loggers due to waves and currents could also lead to false signals in the record. These impediments are subject to further study with appropriate improvement techniques.

The measurement campaigns at at Tambon Tabon and Tambon Rawa allow small sets of 29 and 28 sets of wave spectra, respectively. Examples of them are shown in Figure 4.12

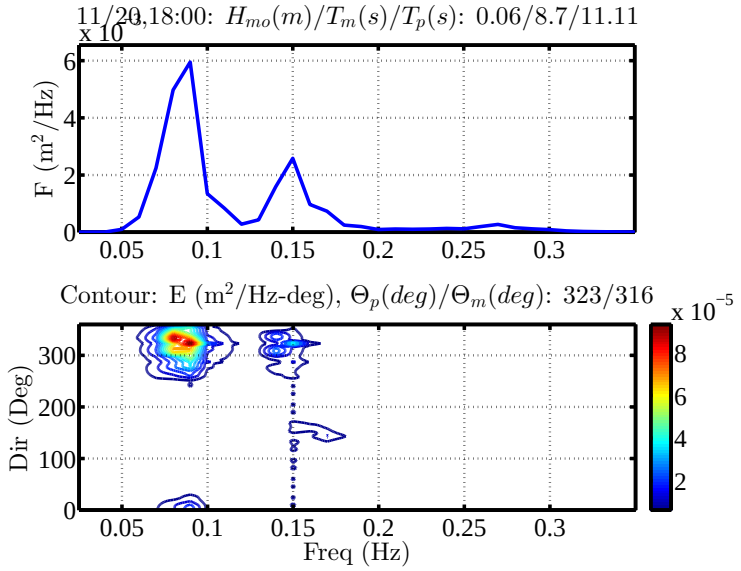

Figure 4.9: Wave spectra obtained offshore of Pakmeng beach on 11/20/2015. Top: wave-frequency spectrum, Bottom: directional wave spectrum.

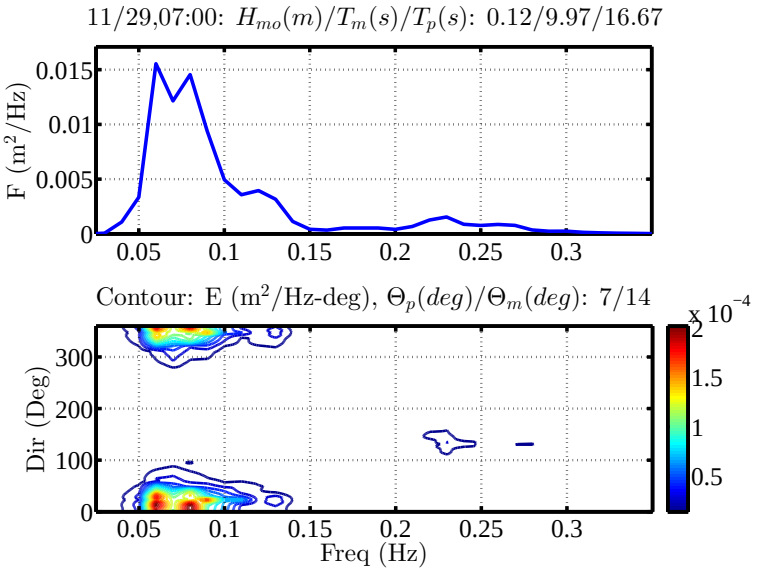

Figure 4.10: Wave spectra obtained offshore of Pakmeng beach on 11/29/2015. See Figure 4.9 for details.

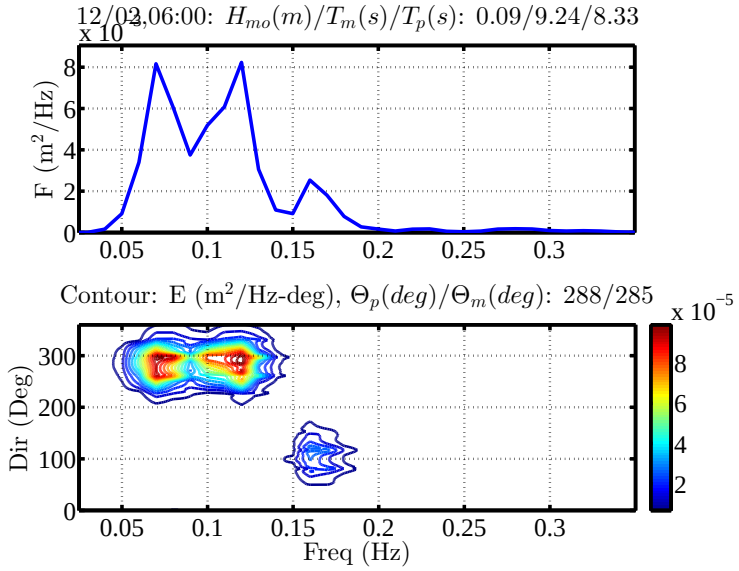

Figure 4.11: Wave spectra obtained offshore of Pakmeng beach on 12/02/2015. See Figure 4.9 for details.

and Figure 4.13 where there can be seen that the components of wave energy appear to have a sharp rising peak and a longer descending tail across the wave frequencies. This spectral shape should be very similar to the forms of wave energy distribution that could be obtained via use of parameterized wave spectra.

For the third location at Thepha Bay, the measurement was performed at two stations which feature different water depths, having the mean values of 4.2 and 5.3 meters. This particular measurement effort took around 7 days with non-directional wave spectra reported hourly. The totals of 166 and 149 records were obtained for the two stations with some examples of each shown in Figure 4.14 and Figure 4.15, i.e. for the shallower(1) and deeper(2) stations, respectively. In both figures, the mean wave spectra calculated for the daytime were compared to those of the nighttime. It can be seen that during the former duration, the site was associated with substantially larger waves. Such a trend was likely subject to seasonal variation of the circulation of winds and waves in this particular region.

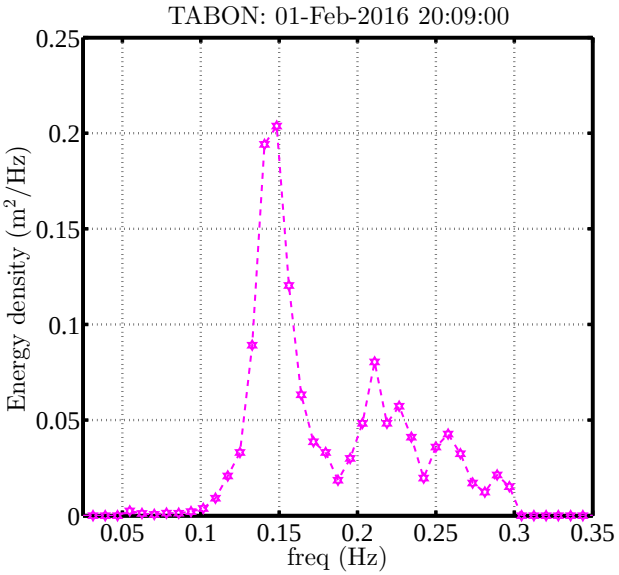

Figure 4.12: Non-directional wave spectrum obtained at Tabon site.

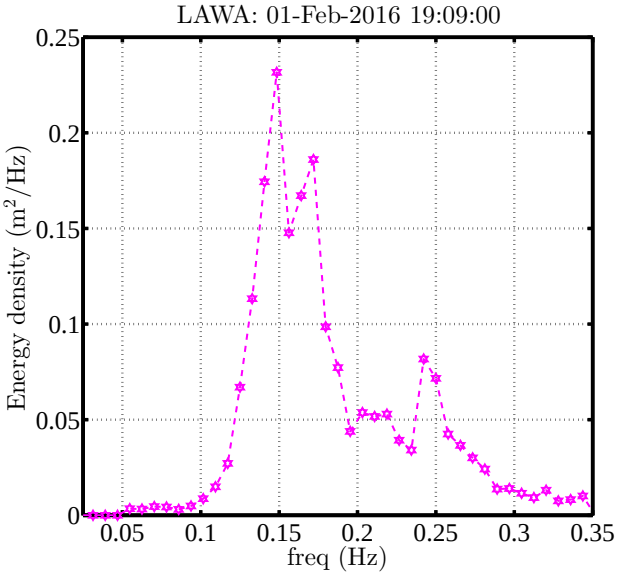

Figure 4.13: Non-directional wave spectrum obtained at Lawa site.

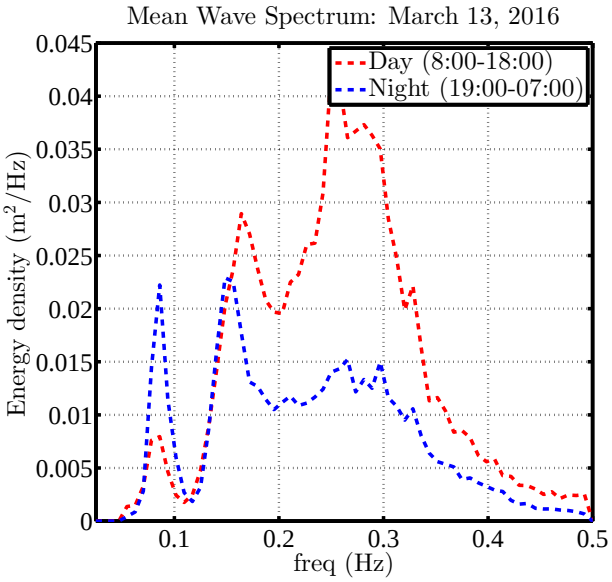

Figure 4.14: Mean wave energy spectra observed at Thepha site(1) during day and night of 03/13/2016.

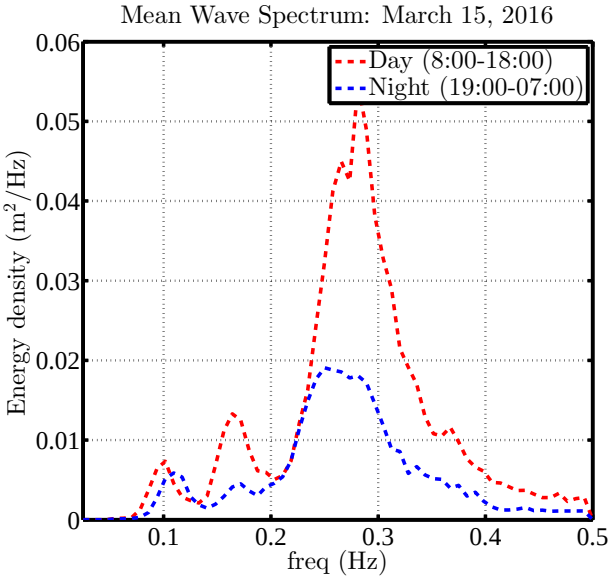

Figure 4.15: Mean wave energy spectra observed at Thepha site(2) during day and night of 03/15/2016.

4.3 Obtaining Data from Other Sources

The spectral wave data obtained from the measurement efforts in this project could be used as part of the verification and validation of the new analytical formulas. In any case, the total availability and coverage of field conditions were fairly limited and therefore external sources of wave data were explored for fulfilling the need. One primary advantage in considering wave data from other sources lies in the fact that almost all such data were already proven to be accurate and precise upon a certain standard. Two major sets of wave data found in the literature and available as online resources were utilized here and they can be described as follow.

The first set of data were from the field measurement by Work (2008) carried out at a site near the Savannah River entrance channel in the State of Georgia, USA, as shown in Figure 4.16. This measurement scheme made use of several Triaxys surface-following wave buoys (Figure 4.17) which reported hourly directional wave energy spectra and wave parameters almost continuously from 2004-2007. The mean water depth at the site is 13.6 m with a tidal range of 2.1 m. For a period of 2.5 months, an acoustic Doppler current profiler (ADCP) was also collocated with the buoy to verify the measured wave spectra. Besides the reliability, the spectral estimates from this work were suitable for testing the new analytical formulas because of the wide variation of their associated relative water depths ($k_p h$).

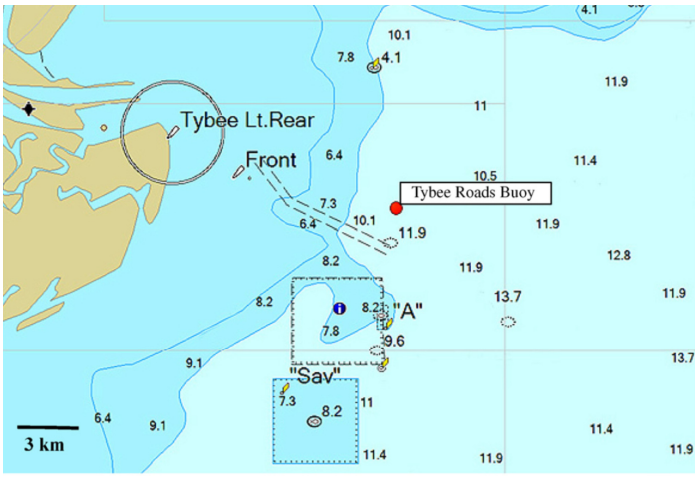

Figure 4.16: Location at which Tybee Road wave bouy was deployed to collect wave spectra.

The other set of wave data were obtained from the National Data Buoy Center (NDBC)

Figure 4.17: Triaxy's solar-powered and telemetry-equipped wave buoy.

of the US National Oceanic and Atmospheric Administration (NOAA), who manages the development, operations, and maintenance of the national data buoy network. At all measurement stations, hourly non-directional wave spectra were recorded and made available to the public routinely. Within this large database, field wave energy spectra available at nine locations along the US Atlantic Coast and the Gulf of Mexico were selected for use for the verification and validation purposes in this research project. Figures 4.18 and 4.19 illustrate examples of wave buoys deployed in each of the two primary locations. Details of all of the measurement stations considered in this study can be found in Table 4.2.

5 Development of Analytical Formulas

As discussed in the previous section, two general options for the estimation of phase-averaged wave parameters are the spectral-based numerical integration and the representative wave approach. The former may also incorporate the use of parameterized wave spectra, but in either case, the numerical scheme involved will not allow a closed-form solution for the problem. Here, a new set of closed-form, analytical solutions are developed for the estimation purpose.

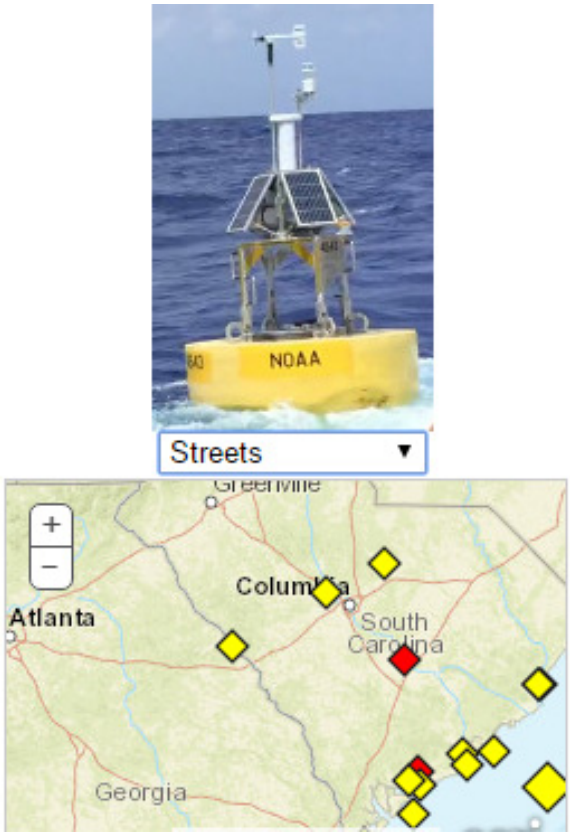

Figure 4.18: Example of NOAA wave buoy deploy in the Atlantic coast of USA (Station ID: 41004).

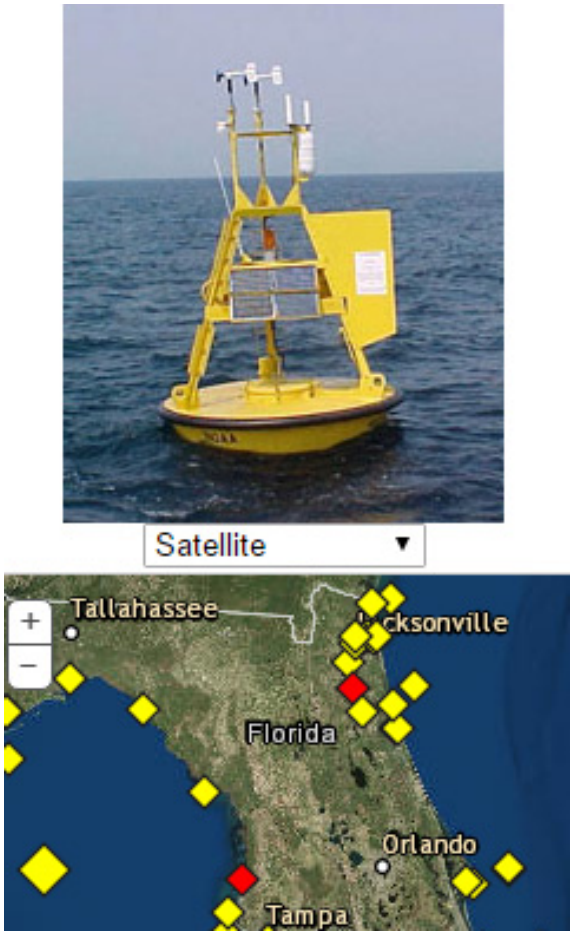

Figure 4.19: Example of NOAA wave buoy deploy in the Gulf of Mexico (Station ID: 42306).

Table 4.2: Details of NDBC stations from which spectral wave data were utilized for validation and verification of the new analytical formulas.

No.	Site Specification			
	Sta. ID.	Position	h (m)	$k_p h$ [-]
1.	41004	32.501N, 79.099W	38.4	0.90-30.6
2.	41008	31.400N, 80.868W	19.5	0.52-15.5
3.	41009	28.522N, 80.188W	40.5	0.85-32.3
4.	41013	33.436N, 77.743W	23.5	0.68-18.7
5.	42012	30.065N, 87.555W	27.7	0.68-24.1
6.	41025	35.006N, 75.402W	68.3	1.53-49.6
7.	42019	27.907N, 95.352W	82.2	2.84-59.8
8.	42020	26.968N, 96.694W	79.9	2.76-52.7
9.	42036	28.500N, 84.517W	50.6	2.07-36.8

5.1 Formulation of Solutions

The proposed solutions were formulated based primarily on physical asymptotes and calculus of the linear wave theory. This preceding introduction of the solutions are focused on non-directional quantities of the target wave parameters, which can be a normal radiation stress in a uni-directional wave field or a total mass flux of random waves. The formulation may start from the spectral estimate expressed earlier in Equations (2.7), which can be rewritten respectively for the wave radiation stress under the given condition as

$$S_{xx} = \int_{f_L}^{f_H} S_\eta(f) \left[\frac{2C_g(f)}{C(f)} - \frac{1}{2} \right] df \tag{5.1}$$

and similarly for the total wave mass flux

$$M_x = \int_{f_L}^{f_H} S_\eta(f)/C(f)\, df \tag{5.2}$$

where f_L and f_H are the lower bound and the upper bound of the frequency range of interest (cutoff frequencies).

An appropriate choice of the parameterized energy spectrum S_η may be selected for the characteristics of a target site. Here, a fully-developed sea in arbitrary water depths is considered with its surface wave energy that distributes following:

$$F_\eta(f) = \vartheta g^2 (2\pi)^{-4} f^{-5} \exp\left(-\frac{5}{4}\left(\frac{f}{f_p}\right)^{-4}\right) . \phi_k(f,h) \tag{5.3}$$

where the multiplier ϕ_k is the depth-dependency factor which approaches unity in deep water condition. Meanwhile, the factor will cause the energy to decrease across the spectrum due to the effect of finite water depth.

In attempt to arrive at a complete set of analytical solutions, the terms in Equations (5.1) and (5.2) must be first rearranged into integrable forms. The attempt can be achieved by use of linear wave theory in which the dispersion relation of waves in a finite water depth is given as

$$k = \frac{\omega^2}{g \tanh(kh)} \tag{5.4}$$

where ω is the angular frequency of the wave ($2\pi f$). This relationship can be substituted into the expression of the depth-dependency factor $\phi_k(f,h)$, given previously in Equation (2.6), to allow its new form that follows

$$\phi_k(f,h) = \left(\frac{\omega^5}{2g^2}\right)\left(k^{-3}\frac{\partial k}{\partial \omega}\right) \tag{5.5}$$

which may still not be evaluated directly since the wave number k in the dispersion relation is not in an explicit form. A possible solution then is to substitute an alternative form of k into Equation (5.5) using an approximate relation suggested by Eckart (1952) that follows

$$k = \frac{u}{h\sqrt{\tanh u}} \tag{5.6}$$

in which u is a non-dimensional factor equal to $(\omega^2 h)/g$. With this substitution, the derivative term in Equation (5.5) can be executed and manipulated to yield

$$\phi_k(f,h) = \tanh(u) + \frac{u}{2}\left[\tanh^2(u) - 1\right] \tag{5.7}$$

This expression can be inserted into Equations (5.1) and (5.2) which would thus be ready for evaluation. Note that explicit forms of the wave celerity factors in the same

equations could also be obtained by use of Eckart's dispersion relation, obeying $C{=}\omega/k$ and $C_g{=}d\omega/dk$. By transforming the integration variable f into the non-dimensional factor u, the two principal equations can be rewritten in the new forms that follow

$$S_{xx} = A_s \left[\int_{u_L}^{u_H} u^{-3} \exp^{-Bu^{-2}} \left(\tanh(u) + \frac{u}{2} \left[\tanh^2(u) \right] \right) du - \int_{u_L}^{u_H} u^{-3} \exp^{-Bu^{-2}} du \right] \tag{5.8}$$

and;

$$M_x = A_m \int_{u_L}^{u_H} u^{-5/2} \exp^{-Bu^{-2}} \left(\frac{\tanh(u) + \frac{u}{2} \left[\tanh^2(u) - 1 \right]}{\sqrt{\tanh(u)}} \right) du \tag{5.9}$$

with the groups of known constants:

$$A_S = \frac{\vartheta h^2}{4\pi}; \qquad A_M = \frac{\vartheta h^{3/2}}{2g^{1/2}}; \qquad \text{and} \qquad B = \frac{5h^2}{4\omega_p^{-4} g^2} \tag{5.10}$$

in which the peak angular wave frequency $\omega_p{=}2\pi f_p$, and the integral limits u_L and u_H are the values of u corresponding to the low and the high frequency cutoffs in the wave spectrum. Noticeably, Equations (5.8) and (5.9) may be arranged in many other forms but they are kept in these formats to enable an execution which are shown next.

5.2 Evaluation for Analytical Expressions

For the wave radiation stress S_{xx}, the two integral terms in Equation (5.8) must be evaluated over the given interval to obtain a closed-form solution. The complexity that exists in the first integral due to the co-existence of the power, the exponential, and the hyperbolic tangent terms (tanh), is first resolved by use of replacement functions obtained from an asymptotic analysis. In part of the analysis, Figure 5.1a illustrates values of the tanh term in Equation (5.8) over a wide range of the non-dimensional factor $u{=}(\omega^2 h)/g$, from which the result clearly shows that

$$\tanh(u) + \frac{u}{2} \left[\tanh^2(u) \right] \approx u, \qquad \text{for} \quad 0 < u \geq u_* \tag{5.11}$$

and

$$\tanh(u) + \frac{u}{2} \left[\tanh^2(u) \right] \approx \frac{u}{2} + 1, \qquad \text{for} \quad u > u_* \tag{5.12}$$

where the threshold factor u_* is simply equal to 2.0 in this case. With these asymptotes and function limits, the first integral in Equation (5.8) may be separated again into three sub-integration terms which lead to a new expression that follows

$$S_{xx} = A_s \left[\int_{u_L}^{u_*} (u^{-2} + u^{-3}) \exp^{-Bu^{-2}} \, du + \frac{1}{2} \int_{u_*}^{u_H} u^{-2} \exp^{-Bu^{-2}} \, du \right] \tag{5.13}$$

These new terms can thus be prepared for an integration by parts and by substitution together with aids of the non-elementary Gauss error function (erf) that is defined in an integral form as

$$\mathrm{erf}(Z) = \frac{2}{\pi} \int_0^Z \exp^{-u^2} \, du \tag{5.14}$$

which subsequently allows an evaluation on Equation (5.13) to yield

$$S_{xx} = \frac{A_s}{4} \sqrt{\frac{\pi}{B}} \left[\mathrm{erf}\left(\frac{\sqrt{B}}{u_L} \right) - \mathrm{erf}\left(\frac{\sqrt{B}}{u_*} \right) \right] + \frac{A_s}{2B} \left[\exp^{(-B/u_H^2)} - \exp^{(-B/u_*^2)} \right] \tag{5.15}$$

which is the final closed-form, analytical solution for the estimation of the wave radiation stress S_{xx} in a random wave field.

A similar approach can be applied on the integral expression of the wave mass flux given earlier in Equation (5.7). In this case, the result from the asymptotic analysis on the associated tanh term is shown in Figure 5.1b which implies that

$$\frac{\tanh(u) + \frac{u}{2} \left[\tanh^2(u) - 1 \right]}{\sqrt{\tanh(u)}} \approx \frac{u}{2}, \qquad \text{for} \quad 0 < u \geq u_* \tag{5.16}$$

and

$$\frac{\tanh(u) + \frac{u}{2} \left[\tanh^2(u) - 1 \right]}{\sqrt{\tanh(u)}} \approx 1, \qquad \text{for} \quad u > u_* \tag{5.17}$$

in which the threshold factor u_* is still equal to 2.0 here. With these asymptotic functions substituted, Equation (5.9) can be rewritten in a new form that follows

$$M_x = A_m \left[\frac{1}{2} \int_{u_L}^{u_*} u^{-3/2} \exp^{-Bu^{-2}} \, du + \int_{u_*}^{u_H} u^{-5/2} \exp^{-Bu^{-2}} \, du \right] \tag{5.18}$$

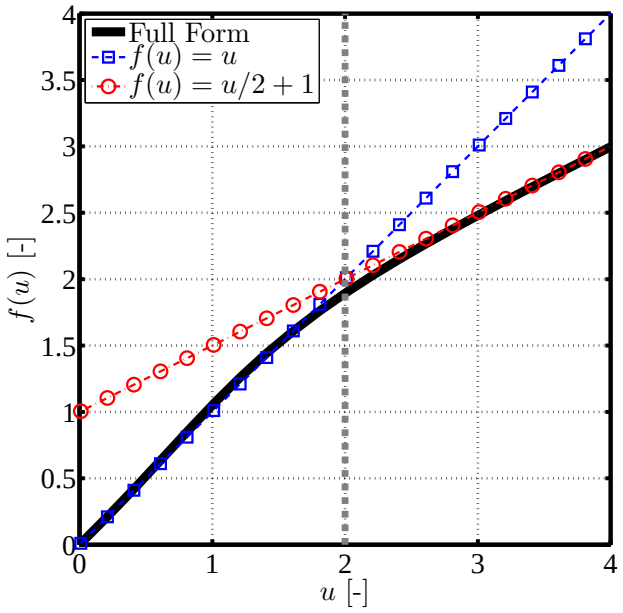

(a) For S_{xx}

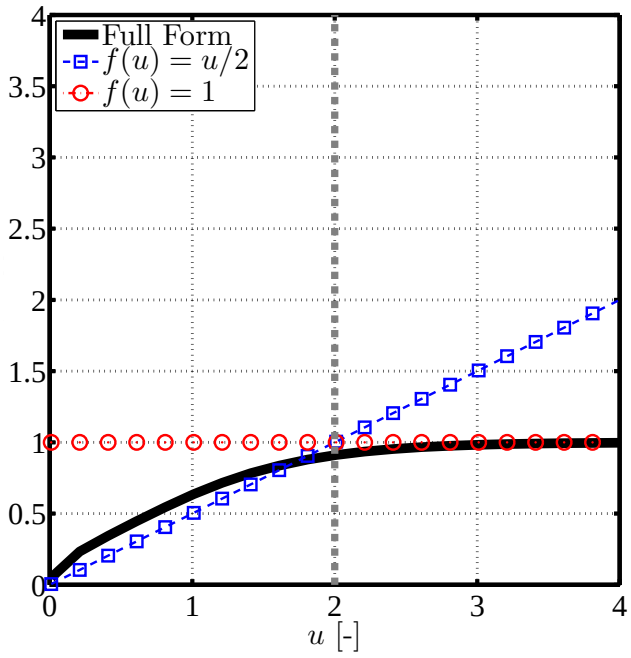

(b) For M_x

Figure 5.1: Exact values of tanh terms and asymptotic values over two function intervals.

Once rearranged for integration by parts and by substitution, Equation (5.18) can be evaluated to yield a final closed-form, analytical solution for the estimation of the total wave mass flux in a random wave field that follows

$$M_x = \frac{A_m}{4B^{1/4}}\left[i\Gamma\left(\frac{1}{4},\frac{B}{u_L^2}\right) - i\Gamma\left(\frac{1}{4},\frac{B}{u_*^2}\right)\right] + \frac{A_m}{2B^{3/4}}\left[i\Gamma\left(\frac{3}{4},\frac{B}{u_*^2}\right) - i\Gamma\left(\frac{3}{4},\frac{B}{u_H^2}\right)\right] \tag{5.19}$$

where $i\Gamma$ is an incomplete gamma function defined such that

$$i\Gamma(Z,u) = \int_0^Z \exp^{-u} u^{Z-1} du \tag{5.20}$$

which represents a definite integral of the gamma function spanning from 0 to the variable limit Z. Both of the new formulas introduced here in Equations (5.15) and (5.19) will be executable on any computing environments in which the error and the gamma functions are built-in routines. In the next section, the new formulas will be investigated for their behaviors focusing on validity in the problem formulation and derivation accomplished here.

6 Verification and Validation

The primary goal in this section is to justify for the validity of the new formulas and, if any, limitation in their applications. Three stages were conducted in the testing which can be described below.

6.1 Comparison to Exact Solutions

The development of the new formulas introduced in Equations (5.15) and (5.19) involves several assumptions and approximations which are to be verified here. The use of Eckart's solution in Equation (5.6), in lieu of the exact dispersion relation in Equation (5.4), needs to be first investigated.

In Figure 6.1, values of the wave numbers k yielded by these expressions are compared in terms of the non-dimensional wave length L/L_o. For the values of kh between $\pi/10$ to π, corresponding to a transitional water depth, the error involved with the approximation is found to be non-zero, but features a very small maximum of around 5%. The magnitude of the error tends to diminish in the lower and upper bounds of kh, suggesting that any misestimation that could arise due to the use of the approximate dispersion relation should be minimal.

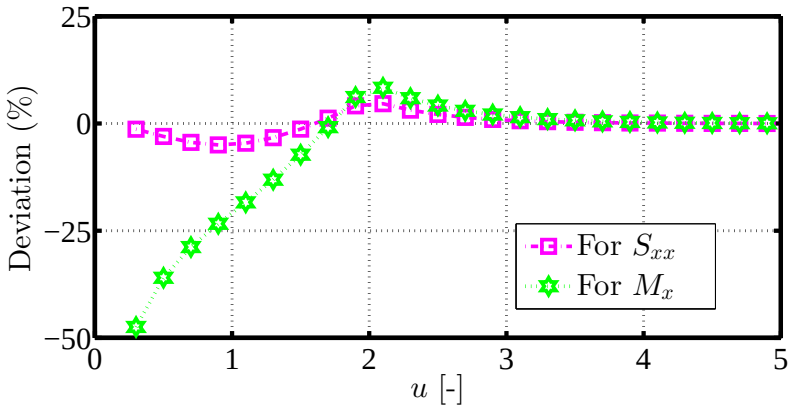

(a) Asymptotic form of tanh term

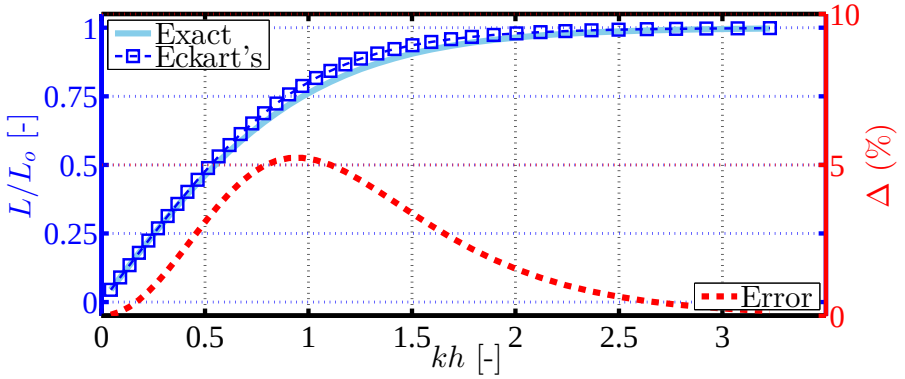

(b) Eckart's dispersion relation

Figure 6.1: Deviations found in the comparisons between exact and approximate terms in the problem formulation. Percent error (Δ) is shown respect to the right axis.

The use of asymptotic relations of the hyperbolic tangent terms (tanh) in Equations (5.11) and (5.12), and Equations (5.16) and (5.17) also needs to be investigated. Based on Figures 5.1a and 5.1b shown previously, the deviations found in the comparison are illustrated quantitatively in Figure 6.2 which shows that the asymptotes adopted in the formulation of S_{xx} is found to be associated with less than 5% in approximation errors. For the asymptotic form for M_x, the possible errors may rise to 50%, but such a high percentage is only found in a low range of the non-dimensional parameter (u<0.5) where the base values from the exact tanh term are very small.

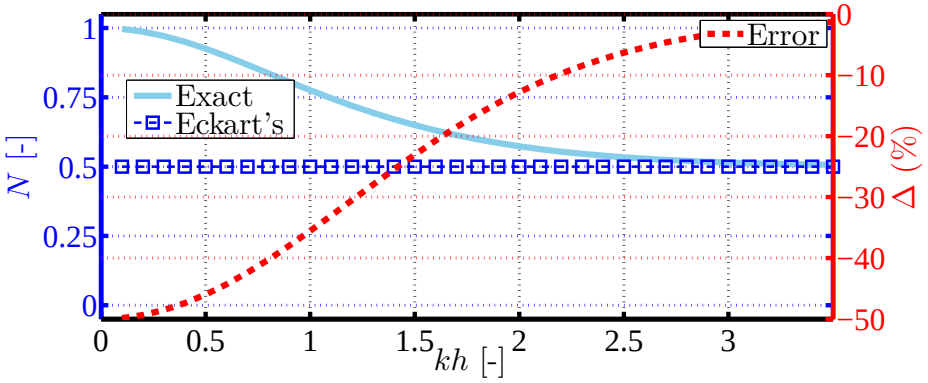

(a) Relative wave celerity

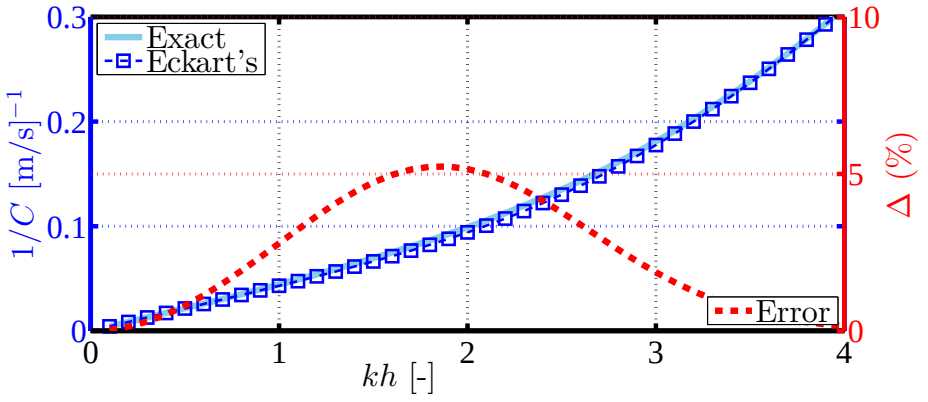

(b) Reciprocal of wave celerity

Figure 6.2: Comparisons between wave celerity parameters computed using exact dispersion relation and Eckart's expression. Percent error (Δ) is shown respect to the right axis.

The investigations here may indicate that the biases involved with individual terms in the development of the new formulas should be limited. Nevertheless, the eventual

impacts on the accuracy and precision of the new formulas still may not be concluded since they will be dependent on both water depth and wave frequencies, and also may cause underestimation or overestimation. The only means to reach a conclusion would be to test the complete forms of the new formulas against spectral wave data which is illustrated in the next section.

6.2 Investigation using Synthetic Wave Data

The primary goal in this section is to find acceptable conditions in which the new analytical formulas could be applied. The use of synthetic wave spectra would suit this need since the control parameters and the wave conditions can be specified in the test. A total of 300,000 synthetic wave spectra, with different peak wave frequencies (f_p) and water depths (h), were generated for use in the test.

Of many physical conditions, the relative water depth (kh) appears to be most critical to the accuracies of the new analytical formulas. In a random wave field, the dominant wave at the peak wave frequency f_p and wave number k_p may be used to define a proximal relative water depth k_ph. Over a wide range of this factor, Figure 6.3 illustrates percent occurrences of the computed errors in the tests for S_{xx} and M_x. The errors are defined according to the differences between the estimated results, from the representative wave approach and the new analytical solutions, and the exact values yielded by the full numerical integration.

In the lower range of $k_ph<\pi/3$ in Figure 6.3a, very high percent occurrences are shown to accumulate around the negative percent errors of 50% which imply that the new solutions tend to underestimate most values of the radiation stress S_{xx} by half their exact values. The representative wave approach, meanwhile, is found to be associated with around 25% overestimation of the parameter. It is in the range of $3\pi/4<k_ph<5\pi/4$ that the new analytical solution appears to outperform the traditional approach.Throughout the evaluation in Figure 6.3, much narrower distributions of the percent occurrences over the errors are always found in the use of the new solution, suggesting that its estimation precision may also be another positive aspect, besides the accuracy.

In the estimation of M_x, Figure 6.3b shows that in the lower range of $k_ph<\pi/3$, both of the techniques tend to underestimate most values of the parameter by -10 to -20%. The performance of the new formula then appears to enhance as the range of k_ph increases towards the deep water limit. An opposite change is found in the estimates yielded by the representative wave approach, as the underestimation arises to -15 to -25%. A narrower distribution of the computed results may be found here in the use of the representative wave

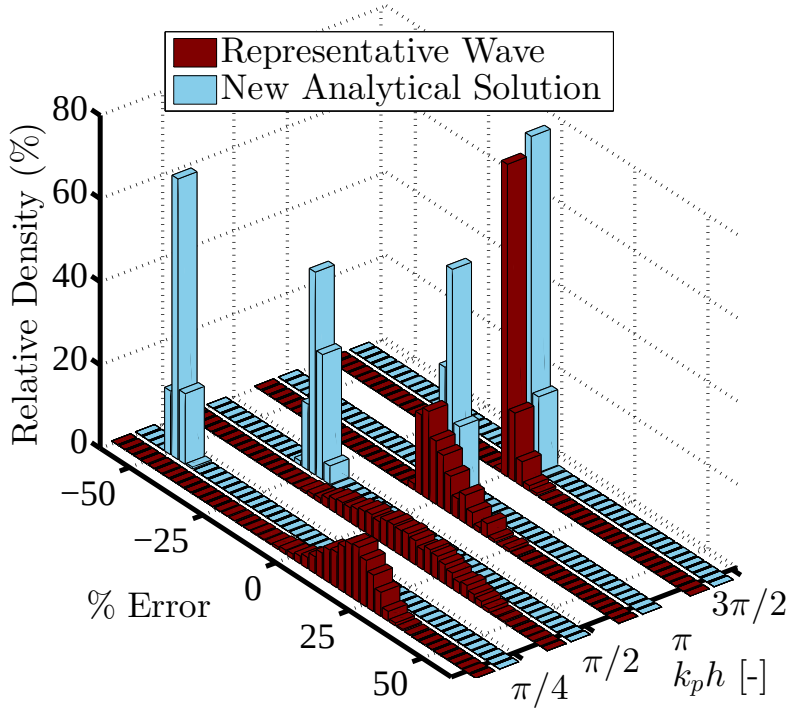

(a) For wave radiation stress S_{xx}

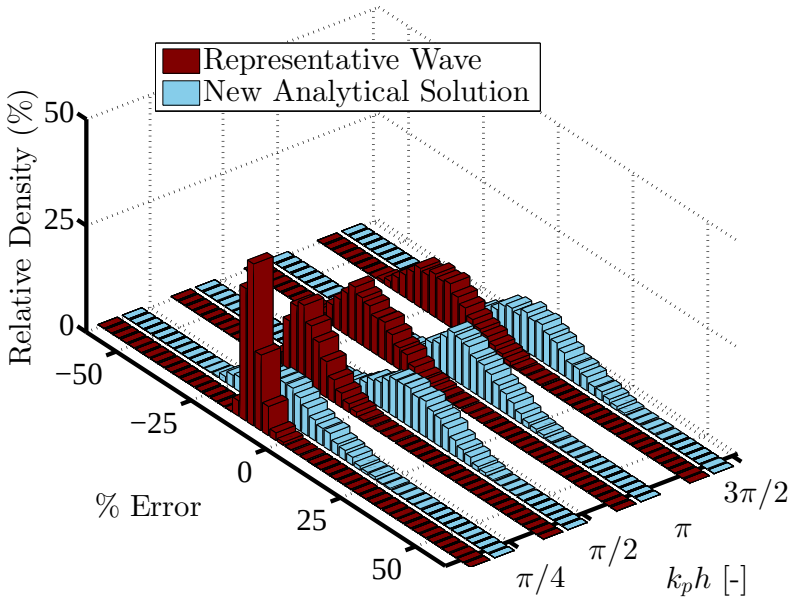

(b) For wave mass flux M_x

Figure 6.3: Relative density of evaluation results based on 16,000 synthetic tests given as functions of estimation errors and relative water depths $k_p h$.

technique, but such superior precision seems to decay quickly with the accuracy in higher ranges of $k_p h$.

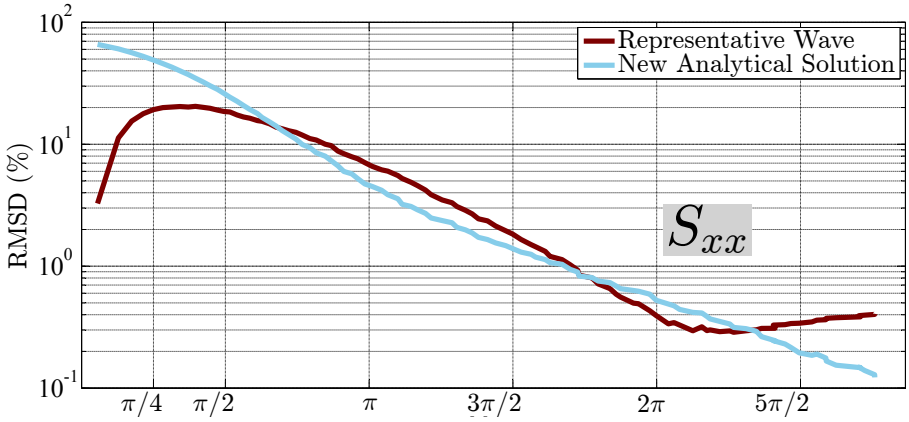

(a) For wave radiation stress S_{xx}

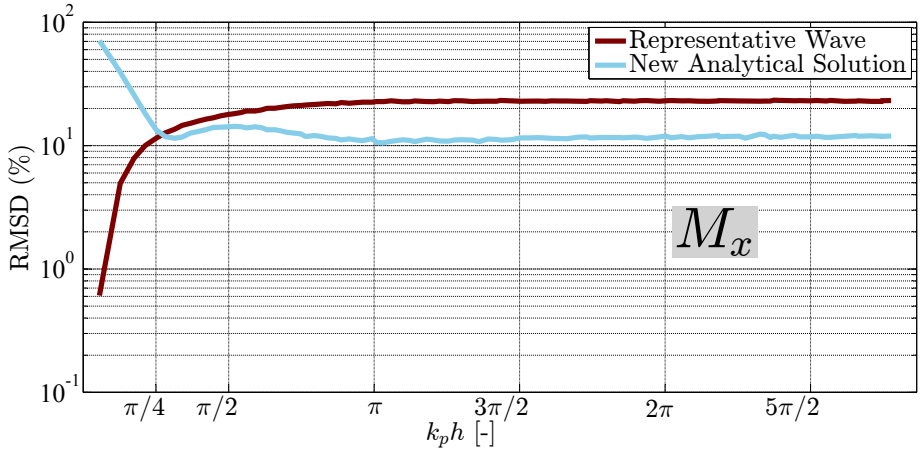

(b) For wave mass flux M_x

Figure 6.4: Root-mean-square deviation (RMSD) found in the synthetic tests on the two different techniques given as a function of relative water depth $k_p h$.

The above findings may confirm that in both of the estimations for S_{xx} and M_x, the new solutions will become a superior option to the representative wave approach under some higher ranges of $k_p h$. To account for both the accuracies and the precisions, certain applicable ranges of the new formulas are justified based on the root-mean-square deviation (RMSD). This statistical factor is defined as the square root of the mean squared error between the estimated and the exact numerical values. Figure 6.4 shows the values of

RMSD associated with the estimates, yielded by the two different techniques. Note that the plotted lines are not perfectly smooth due to the systematic randomness in the synthetic data.

In Figure 6.4a, the new formula for S_{xx} is associated with a substantial deviation in the lower range of k_ph, which was found earlier in Figure 6.3a to be an underestimation. As the limit of k_ph approaches $\pi/2$, such deviations from the two different techniques become more comparable before the new solution appears to provide more accurate estimates for greater values of k_ph. This comparison reveals that the new formula for S_{xx} should be suitable for use when the factor k_ph is greater than $\pi/2$.

In Figure 6.4b, the RMSD values yielded by the two different techniques in the estimation of M_x are compared. For $k_ph<\pi/4$, the new analytical solution has a very substantial deviation of up to 80%. For higher values of k_ph, the new solution exhibits a superior performance to the representative wave approach, which is especially clear when the factor k_ph is greater than $\pi/2$. This clarity suggests that the applicable range of the new analytical formula for M_x should be identical to that of the new formula of S_{xx}, defined at $k_ph>\pi/2$.

6.3 Investigation against Nearshore Wave Buoy Data

The performances of the new formulas are reexamined here based on wave data from an in-situ wave measurement device. The primary objectives are to confirm the applicable ranges of the formulas defined previously as a function of k_ph, and to investigate possible sensitivities of the formulas on the variation of sea state and energy distribution in the wave field.

More than 16,000 hourly records of spectral waves achieved by Work (2008) were utilized for this validation. Using the numerical approach, best estimates of the wave radiation stress (S_{xx}) and the wave mass flux (M_x) were computed from the measured wave spectra. These estimates were then compared to the values yielded by the new analytical solutions and the representative wave approach from which the mean absolute errors are shown for many ranges of k_ph in Figure 6.5a. For k_ph below the applicable limit at $\pi/2$, the estimation errors on S_{xx} from the two techniques are opposite, with the new analytical solution tending to underpredict the parameters.

Beyond the threshold, such an underestimation decreases and the new formula appears to allow more accurate results than the single wave approach. This tendency can be confirmed as both of the percent errors and their standard deviations decrease significantly at higher ranges of k_ph. Note that there are few ranges of k_ph in which the representative

approach seems to provide slightly smaller errors, but only because its overestimation trend starts to change to an underestimation. This fact can be observed in Figure 6.5a at the value of $k_ph \approx 3\pi/4$ with the computed errors progressing from the positive to the negative sides of the results.

In Figure 6.5b, the magnitudes of the wave mass flux (M_x) below the limit of $k_ph < \pi/4$ were found to be underestimated by both of the estimation techniques. As the value of k_ph increases beyond $\pi/2$, the negative deviation in the new solution diminishes quickly and tends to neutralize to a mean value of zero. This tendency occurs according to the fact that more neutral results from the new solution, while featuring smaller mean absolute errors, initiate a wider total range of errors as they are associated with comparable magnitudes of underestimation and overestimation as illustrated in Figure 6.5b.

The new analytical solutions can be verified according to the results shown in Figure 6.5, but their estimation performances could also be dependent on some other factors. Therefore, three additional parameters commonly used to describe the random sea are investigated for their possible influences on the computed values of S_{xx} and M_x. One is the relative wave height, expressed simply as the ratio between the mean wave height and the water depth (H/h). This parameter behaves like an indicator for the measure of water depth, but it is classified on the basis of the wave height instead of the peak wave number adopted in the factor k_ph.

Another influential parameter is for the quantification of the overall steepness of the random sea, defined as the spectral steepness factor S_p that follows:

$$S_p = 2\pi \left(\frac{H_{m0}}{gT_p^2} \right) \tag{6.1}$$

where H_{m0} and T_p are the spectral-based significant wave height and the peak wave period, in that order. The relativity between these two physical wave parameters indicates a non-dimensional steepness of the wave field, interpreted more straightforwardly as a wave height to wave length ratio.

The other testing factor is for the measure of the relative width of the spectrum, or the degree at which the energy is distributed over the entire frequency bands. According to Longuet-Higgins (1975), this characteristic may be quantified by use of the spectral width parameter ν defined as

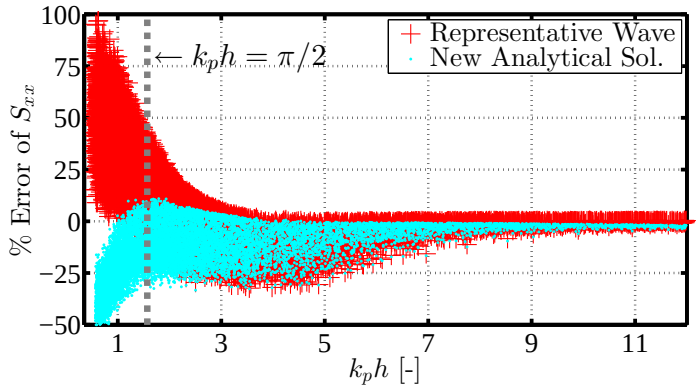

(a) For wave radiation stress S_{xx}

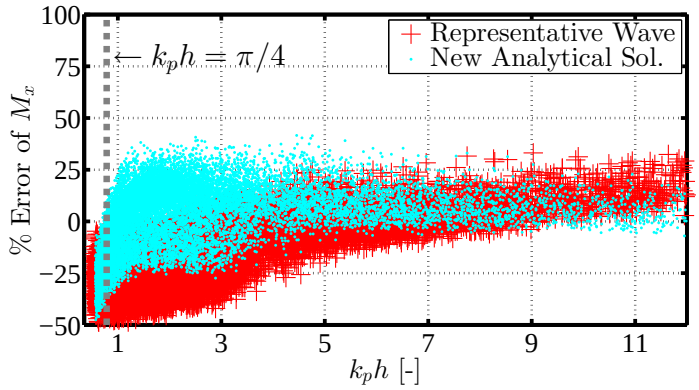

(b) For wave mass flux M_x

Figure 6.5: Estimation errors as a function of relative water depth $k_p h$ found in the validation of the two techniques against in-situ wave buoy data.

$$\nu = \left(\frac{M_0 M_2}{M_1^2} - 1 \right)^{1/2} \tag{6.2}$$

in which M_n is the n^{th} moment of the wave energy spectrum. Typical values of ν may span between 0.3 and 0.5 in the TMA and JONSWAP parameterized wave spectra, with a similar range also found in most wind-sea dominated field wave spectra (e.g. Soares and Carvalho 2003).

The three hyphothesized parameters were first computed for all of the available wave spectra. The errors involved in the two estimation techniques are subsequently related as functions of these influential parameters as shown in Figure 6.6. The sensitivities due to the relative wave height (H/h) are depicted in Figures 6.6a and 6.6b for S_{xx} and M_x, respectively. In overall, both of the new solutions appear to be more accurate in the lower range of H/h, simply because of the fact that most smaller values of H/h are found under a deeper water condition, i.e. in analogy to possessing large values of $k_p h$.

For both S_{xx} and M_x, the two estimation techniques are found to produce certain errors that form a concave-up parabola over the horizontal axis of the steepness factor S_p as shown in Figures 6.6c and 6.6d. Those greater errors in the lower and the upper ranges of S_p are believed to generally occur with some of the measured wave spectra that feature irregular energy distributions over the frequency bands. Some higher values of S_p could be associated with energy spectra in which high-frequency waves are dominant thus resulting in a shorter and steeper wave field in overall. An opposite tendency can be true in the cases with lower values of S_p.

The sensitivities of the two techniques on the relative width of wave spectra ν are investigated in Figure 6.6e and 6.6f, for the estimations of S_{xx} and M_x, respectively. In both cases, the estimation errors are clearly found to rise as the values of ν increases, which is a scenario when the overall energy distributes more widely over the frequency bands. This variation found may lead to a straightforward conclusion that the estimation errors should be proportional to the spectral bandwidth.

In the meantime, the performances of both of the estimation techniques seem to decline for a very high range of ν. For the values of ν beyond 0.55, the representative wave approach may appear to become the superior estimation option but in fact neither of the techniques should be employed because their underlying assumptions would already be violated. The spectra will not be narrow-banded, nor could they be formed via the parameterization.

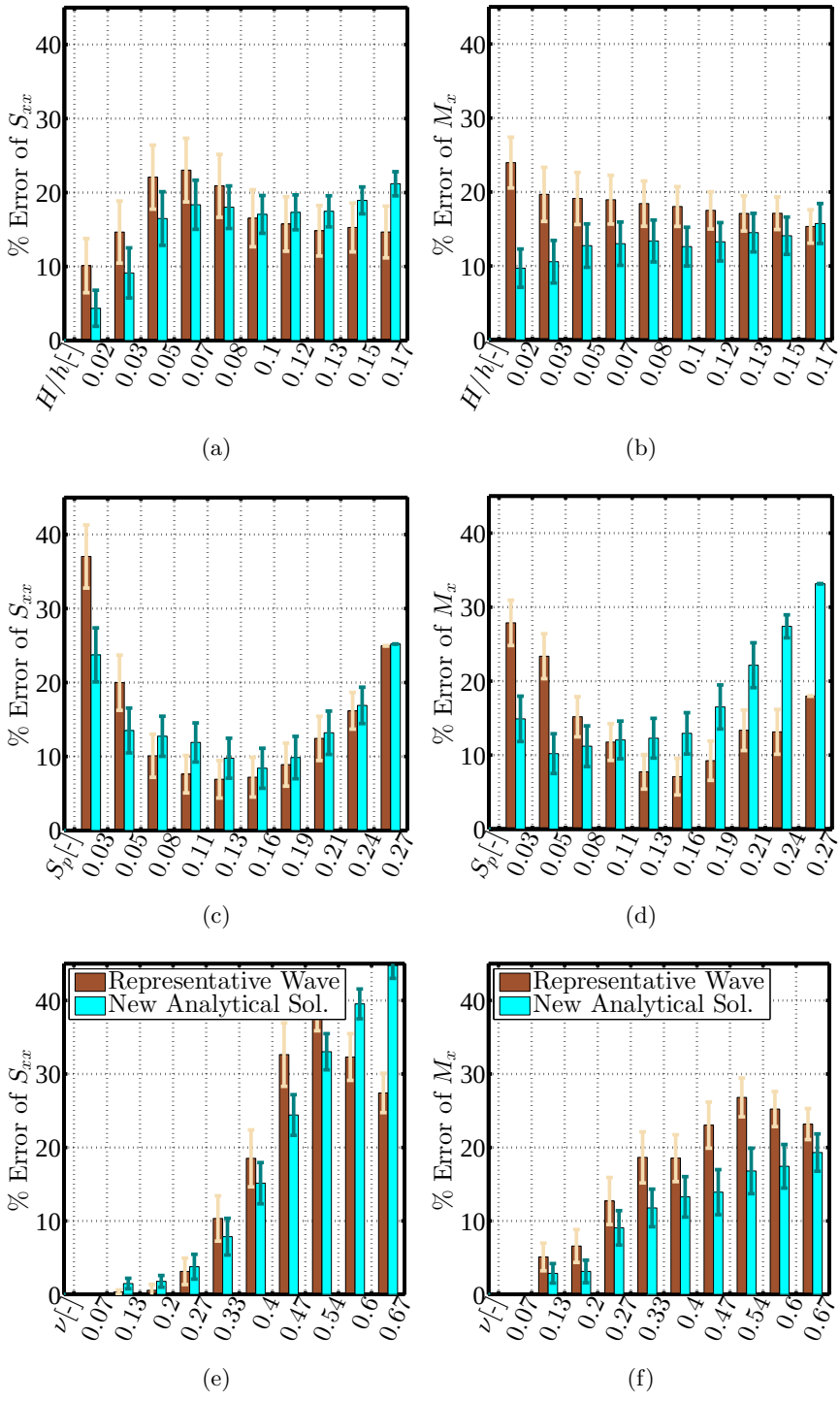

Figure 6.6: Variation of the estimation errors found in the sensitivity tests based on three influential spectral factors. Top (a,b) for H/h; middle (c,d) for S_p; bottom (e,f) for ν.

Several conclusions could be drawn from the above verification. While the new formulas seem to be somewhat sensitive to the relative spectral wave height (H/h) and the sea steepness (S_p), they are much more influenced by the relative water depth (k_ph). In terms of the distribution of spectral wave energy, unsurprisingly, the new solutions seem to perform better when applied to a wave field that resembles their prototype parameterized wave spectrum. The spectral width factor ν could be adopted as an indicator for this particular condition.

6.4 Investigation based on Offshore Wave Buoy Data

To reassure their performances under various field conditions, the new analytical formulas are verified again here based on field wave energy spectra available through the National Data Buoy Center (NDBC) of which the details are given earlier (Table 4.2). For the total of 7,000 hourly spectral wave records from each site, the best estimates of S_{xx} and M_x yielded by the exact numerical integration were treated as benchmark for the evaluation of the representative wave approach and the new analytical formulas.

For clarity, the estimation results were classified into two separate groups. One includes those from Stations 1 to 5 which also see the lower intermediate water depth ($k_ph>\pi/4$), while the other includes those from Stations 6 to 9 with the upper intermediate water depth and beyond only ($k_ph>\pi/2$). Three quantitative factors based on the results from the two techniques were inter-compared including the mean absolute error, the estimation bias, and the standard deviation of the errors given as percentage of the mean. Residuals of all these factors from the intercomparison, taking the new solution results as minuends, are summarized in Table 6.1.

The results from the first group of stations with shallower water waves show that the values of S_{xx} from the new solutions tend to be slightly underestimated, but an opposite trend is found for those from the representative wave approach. A more careful consideration on the resulting indicators can reveal that the new solution should allow the estimation results of S_{xx} that are associated with substantial smaller absolute errors and scatterers. All of these residuals featuring negative values in the estimation of S_{xx} for Stations 1 to 5 could confirm the superiority of the new analytical solution over the representative wave approach.

In the cases of Stations 6 to 9, both of the estimation techniques seem to allow very accurate results but the new analytical solution still appears to be the superior option in terms of estimation precision. This tendency can be confirmed based on the standard

Table 6.1: Residuals of statistical indicators found in the comparison between the results from the two different techniques. Note: the residuals were computed based on absolute values with those of the new solutions taken as minuends.

No.	**Sta. ID.**	**Radiation Stress:** S_{xx}			**Mass Flux:** M_x		
		Δ BIAS [-]	Δ Error (%)	Δ Std. (%)	Δ BIAS [-]	Δ Error (%)	Δ Std. (%)
1.	41004	-0.03	-1.86	-12.19	-0.10	-9.83	-6.51
2.	41008	0.00	-6.05	-12.60	-0.05	-7.21	-0.12
3.	41009	-0.06	-1.62	-14.71	-0.18	-10.72	-12.97
4.	41013	-0.02	-5.42	-10.75	0.00	-7.01	4.52
5.	42012	-0.01	-0.14	-5.85	-0.20	-10.93	-9.39
6.	41025	-0.02	0.04	-7.21	-0.10	-8.61	-7.42
7.	42019	0.00	0.52	0.10	-0.18	-10.86	-10.87
8.	42020	0.00	0.46	0.28	-0.20	-12.69	-11.40
9.	42036	-0.01	0.97	-2.55	-0.14	-9.04	-12.82

deviations in Table 6.1 which could be up to 7 percents higher in the use of the representative wave approach. A common scenario for this case is when the characteristics of the sea discourage the narrow-banded assumption thus disallowing the use of any nominal wave for a precise description of the wave field.

The resulting estimates of the wave mass flux (M_x) are also compared in Table 6.1. For the first group of data sets, the results clearly show that the representative wave approach tends to underestimate the results while the new analytical solution is associated with an overestimation. The former tendency appears be somewhat more significant and could be confirmed to lead to up to 20% higher bias than the possible overestimation in the new solution. The estimation accuracy may also be compared more directly on the mean absolute errors which are around of 7-10% smaller in the use of the new analytical formula.

The resulting standard deviations of the errors, which measure the precision, also appear to be lower by up to 13% for the new analytical solution. The same type of estimates for the deeper measurement stations are found to feature a very similar trend compared to that of the shallower stations. Such an agreement between the two physical site conditions can be confirmed by the numbers analyzed in Table 6.1, all of which appear in the same sign within a comparable range of magnitudes.

All of the encouraging findings from the above tests may confirm the validities and

capabilities of the new analytical formulas. For the wave radiation stress, the new solution was proved to allow accuracy and precision both higher than the traditional representative wave approach, especially in the tests that included wave data from transitional water depths. Such a potential may become obscured under a deeper water condition only because the two different techniques already produce very small estimation errors. The superior performance of the new solution for the wave mass flux M_x, meanwhile, appear to be unanimous in any conditions, provided it is applied under the applicable range of $k_p h > \pi/4$.

7 Conclusion

Momentum and mass balance over a wave train play an important role in the study of surface water waves as it allows an explanation for many essential processes in the sea. Wave radiation stress (S_{xx}) and wave mass flux (M_x) are two dynamic parameters that fulfill the description. To determine these parameters, two traditional methods are available including a numerical means applied on a full wave energy spectrum, and a representative wave approach which relies only on some nominal parameters of the wave field. The advantages of these two options are interchanging between the ability to consider all individual random waves and the provision of closed-form solutions for analytical application.

The present research project attempts to develop a new set of formulas for the estimation of S_{xx} and M_x while optimizing the preferable capability from each of the traditional options. The problem formulation starts by substituting parameterized wave spectra for an alternative description of the random wave field. The complex non-integrable expressions of both S_{xx} and M_x are first relaxed by use of a simplified wave dispersion relation. Physical asymptotes and calculus of the linear wave theory are then applied as two major keys in the derivation of the new analytical formulas.

The formulation and the derivation were carefully investigated to reveal that the simplification and asymptotic relation may lead to non-zero but apparently insignificant biases on the resulting parameters. A comprehensive set of synthetic wave data were generated to verify the complete formulas and to find their applicable ranges over which their estimation performances are greater than those of the representative wave approach. These ranges are defined on the basis of the proximal water depth factor $k_ph>\pi/2$ and $k_ph>\pi/4$ for the formulas of S_{xx} and M_x, respectively.

The new formulas and their sensitivities on various sea states were examined using reliable in-situ wave spectra. At a first glance, the relative spectral wave height (H/h) and the sea steepness (S_p) were observed to be sensible factors but were, in fact, co-influenced by the relative water depth (k_ph). The new solutions appear to work best in some lower ranges of H/h and S_p which are already confined within the applicable limits based on k_ph. Meanwhile, the most influential sea characteristic seems to be the spreading of wave energy indicated by the spectral width factor ν. Despite such an influence, for more than 90% of the applicable test cases, the new solutions still provided more accurate estimates than the representative wave approach.

The new formulas were once again validated against nine independent sets of wave

energy spectra obtained by the National Data Buoy Center (NDBC) along the US Atlantic Coast and the Gulf of Mexico. The new formula of S_{xx} was proved to allow more accurate and precise estimates than the representative wave approach. This fact is applied in both transitional and deep water conditions but is especially clear in the former. For the estimation of M_x, the superior performance of the new solution appear to be unanimous in either condition. Based on the mean errors compared, overall accuracy improvements of around 5% and 10% could be expected for the new formulas of S_{xx} and M_x, respectively. The standard deviations associated with the errors were also around 10% smaller for both of the new formulas which indicate a significant enhancement in the estimation precision.

A simple explanation is possible for the superiority of the new analytical formulas over the traditional approach. When the full numerical method directly accounts for all random waves, the implicit cross-spectrum integration in the new formulas also serves to imitate the process via the use of a parameterized wave spectrum. The actual and the parameterized spectra may not be perfectly matched but they always share some standard characteristics that are influential to the estimation of the wave parameters, including the spectral shape and the higher and lower bounds of the wave frequencies, for example. The representative wave approach, meanwhile, only accounts for single values of wave height and wave period based on the assumption of a narrow-banded sea. It is this reliance on such an ideal condition that suppresses the capability of the approach for practical application on in-situ wave spectra with much uncertainty and randomness.

The theoretical development achieved in this study is expected to be beneficial to the study of surface water waves. The new formulas that appear in closed analytical forms should be easily comprehended and applied by practitioners in coastal and ocean engineering. The enhancement in the estimation accuracy and precision should encourage the new formulas to be a key upgrade in any modeling tools for wave hydrodynamics and ocean circulation. A research work in progress is aimed at extending the applicability range of the new formulas. Besides, the possibility to arrive at some newer solutions is being explored for other important phase-averaged wave parameters, especially those related to wave energy and wave power.

References

Bouws, E., Gunther, H., Rosenthal, W., Vincent, C. L., 1985. Similarity of the wind wave spectrum in finite depth water 1. Spectral Form. Journal of Geophysical Research-Oceans 90 (1), 975–986.

Cambazoglu, M. K., Haas, K. A., 2011. Numerical modeling of breaking waves and cross-shore currents on barred beaches. J. of the Waterway Port Coastal and Ocean Eng. 137 (6), 310–323.

Capon, J., 1969. High-resolution frequency-wavenumber spectrum analysis. Proceedings of the IEEE 57 (8), 1408–1418.

Davidson-Arnott, R., 2010. Introduction to coastal processes and geomorphology. Cambridge University Press, UK.

De Vriend, H. J., Stive, M. J. F., 1987. Quasi-3D modelling of nearshore currents. Coastal Eng. 11 (5-6), 565–601.

Dean, R. G., Dalrymple, R. A., 1991. Water Wave Mechanics for Engineers and Scientists. Adv. Series on Ocean Eng., Vol. 2. World Scientific, Singapore.

Ding, Y., Wang, S. S. Y., Jia, Y. F., 2006. Development and validation of a quasi-three-dimensional coastal area morphological model. J. of the Waterway Port Coastal and Ocean Eng. 132 (6), 462–476.

Eckart, C., 1952. The propagation of gravity waves from deep to shallow water. In: Gravity waves, National Bureau of Standards Circular 521. Vol. 1. pp. 165–173.

Feddersen, F., 2004. Effect of wave directional spread on the radiation stress: comparing theory and observations. Coastal Eng. 51 (5), 473–481.

Haas, K. A., Svendsen, I. A., Haller, M. C., Zhao, Q., 2003. Quasi-three-dimensional modeling of rip current systems. J. Geophys. Res. 108 (C7), 3217–3238.

Haas, K. A., Warner, J. C., 2009. Comparing a quasi-3D to a full 3D nearshore circulation model: SHORECIRC and ROMS. Ocean Modelling 26 (1-2), 91–103.

Hasselman, K., Barnett, T. P., Bouws, E., Carlson, D. E., Hasselmann, P., 1973. Measurements of wind-wave growth and swell decay during the joint north sea wave project (JONSWAP). Deutsche Hydrographische Zeitschrift 8 (12).

Holthuijsen, L. H., 2007. Waves in oceanic and coastal waters. Cambridge University Press, UK.

Hughes, S. A., 2004. Estimation of wave run-up on smooth, impermeable slopes using the wave momentum flux parameter. Coastal Eng. 51 (11), 1085–1104.

Li, M., Fernando, P. T., Pan, S., O'Connor, B. A., Chen, D., 2007. Development of a quasi-3D numerical model for sediment transport prediction in the coastal region. J. of Hydro-Environment Res. 1 (2), 143–156.

Longuet-Higgins, M., 1975. On the joint distribution of the periods and amplitudes of sea waves. J. of Geophysical Res. 80 (18), 2688–2694.

Longuet-Higgins, M., Stewart, R. W., 1964. Radiation stress in water waves, a physical discussion with applications. Deep Sea Res. 11, 529–563.

Pawka, S. S., 1983. Island shadows in wave directional spectra. Journal of Geophysical Research 88 (C4), 2579–2591.

Pierson, W. J., Moskowitz, L., 1964. Proposed spectral form for fully developed wind seas based on similarity theory of S. A. Kitaigorodskii. Journal of Geophysical Research 69 (24), 5181–5190.

Rakha, K. A., 1998. A quasi-3D phase-resolving hydrodynamic and sediment transport model. Coastal Eng. 34 (3-4), 277–311.

Soares, C. G., Carvalho, A., 2003. Probability distributions of wave heights and periods in measured combined sea-states from the Portuguese coast. J. of Offshore Mechanics and Arctic Eng. 125 (3), 198–204.

Srisuwan, C., Work, P. A., 2015. Beach profile model with size-selective sediment transport. II: Numerical modeling. J. of Waterway, Port, Coastal, and Ocean Eng. 141 (2), 04014033.

Stive, M., Wind, H. G., 1982. A study of radiation stress and set-up in the nearshore region. Coastal Eng. 6 (1), 1–25.

Svendsen, I. A., 2006. Introduction to Nearshore Hydrodynamics. Adv. Series on Ocean Eng. World Scientific, Hackensack, NJ.

Tayfun, M. A., 1986. On narrow-band representation of ocean waves: 1. Theory. J. of Geophysical Res.: Oceans (1978–2012) 91 (C6), 7743–7752.

Wang, B., Chadwick, A. J., Otta, A. K., 2008. Derivation and application of new equations for radiation stress and volume flux. Coastal Eng. 55 (4), 302–318.

Wargula, A., Raubenheimer, B., Elgar, S., 2013. The effects of wave forcing on circulation at New River Inlet, NC. Proceedings of Coastal Dynamics 2013, 1871–1880.

Work, P. A., 2008. Nearshore directional wave measurements by surface-following buoy and acoustic doppler current profiler. Ocean Eng. 35 (8-9), 727–737.

Appendix I: Output from the Research Project

Output จากโครงการวิจัยที่ได้รับทุนจาก สกว.

1. ผลงานตีพิมพ์ในวารสารวิชาการนานาชาติ

   “Srisuwan, C., Rattanamanee, P., Rattanapitikon, W. (2017). Analytical Formulas for Estimation of Phase-Averaged Parameters of Random Waves. Ocean Engineering (ELSEVIER), Vol. 133, pp. 22-35.”

   Database: ISI Web of Science

   Quartile: 1st (Marine Engineering)

   5-Year Impact Factor: 2.184

   Link: http://www.sciencedirect.com/science/article/pii/S0029801816306114

2. การนำผลงานวิจัยไปใช้ประโยชน์ ☑ **ด้านวิชาการ**

   โดย 1) Department of Civil Engineering, Faculty of Engineering, Prince of Songkla University.

   This research project has produced a final result in terms of new theoretical formulas which can be employed in the estimation of important surface wave parameters in the coastal ocean. These formulas as well as important research findings have now been added to the graduate-level lecture at the Department of Civil Engineering, Prince of Songkla University. The courses in which these new contents appear include: 220-540 Linear Water Wave Mechanics, and 220-543 Nearshore Hydrodynamics.

   และโดย 2) All interested parties in the field of coastal and ocean engineering.

   The new body of knowledge and the new analytical tool accomplished in this research has led to a production of an article titled “Analytical formulas for estimation of phase-averaged parameters of random waves”. This article has been published in Ocean Engineering (Vol. 133) which is ranked in the 1st quartile as being one of the most prestigious journals in the subject field of Marine Engineering. The article is available online in the ScienceDirect and ISI Web of Science databases. All interested persons from anywhere can make the most of all of the outputs from this research project.

Appendix II: Article Published in Ocean Engineering

Ocean Engineering 133 (2017) 23–35

Contents lists available at ScienceDirect

Ocean Engineering

journal homepage: www.elsevier.com/locate/oceaneng

Analytical formulas for estimation of phase-averaged parameters of random waves

Chatchawin Srisuwan[a,*], Payom Rattanamanee[a], Winyu Rattanapitikon[b]

[a] Department of Civil Engineering, Faculty of Engineering, Prince of Songkla University, Hat Yai 90112, Thailand
[b] Sirindhorn International Institute of Technology, Thammasat University, Pathum Thani 12121, Thailand

ARTICLE INFO

Keywords:
Ocean surface waves
Wave radiation stress
Wave mass flux
Phase-averaged wave parameters
Wave energy spectra
Parameterized wave spectra

ABSTRACT

New analytical formulas for the estimation of wave radiation stress and wave mass flux are developed in this study based on asymptotic analysis of linear wave theory with the aid of non-directional parameterized wave spectra. Verification against synthetic wave data shows that the new formulas can allow up to 10% more accurate results compared to the use of the traditional representative wave approach. Sensitivity analysis based on reliable wave buoy data reveals that the performance of the new formulas may vary by up to 20% depending on the relative wave height, wave steepness, and spectral width. For a common sea state dominated by wind-induced waves, the formulas are most sensitive to the relative water depth $k_p h$ and their best applicable range is in upper transitional to deep water conditions ($k_p h \geq \pi/2$). The formulas were finally validated against nine independent sets of field wave spectra to reassure their superiority over the representative wave approach. The validation confirms that the new formulas can offer up to 10% and 15% improvements in terms of the estimation accuracy and the estimation precision, respectively.

1. Introduction

The balance of momentum and fluid mass over a series of water waves is typically described in terms of wave radiation stress and wave mass flux. These important wave parameters allow an explanation for many essential phenomena in the sea, including wave setup and setdown, undertow, longshore current, edge waves, and shear waves (e.g. Svendsen, 2006; Davidson-Arnott, 2010). An effective means to determine the parameters is required at a wide range of water depths. Accurate offshore estimates of the parameters are crucial for the preparation of wave climatology data which serve as numerical model inputs. These wave forcing terms are also important in the description of wave transformation towards the shoreline (e.g. Hughes, 2004; Wargula et al., 2013). The capability to estimate the wave radiation stress and wave mass flux therefore plays a very important role in many types of ocean circulation and coastal morphodynamic models (e.g. DeVriend and Stive, 1987; Haas et al., 2003; Srisuwan and Work, 2015).

In a phase-averaged sense, the radiation stress and wave mass flux are estimated per their total quantities over the wave period. Some advanced wave theories may permit the estimation on a phase-resolving, wave-by-wave basis (e.g. Rakha, 1998; Li et al., 2007). The intra-wave approach may enable a direct simulation of non-linear wave phenomena, but sometimes dynamic processes that involve uncertainty and randomness still cannot be described clearly enough for its practical implementations. The use of the phase-averaged estimation has been attempted in many research efforts to show that such an approach can lead to satisfactory modeling results under a wide range of wave conditions (e.g. Ding et al., 2006; Haas and Warner, 2009; Cambazoglu and Haas, 2011).

For monochromatic sinusoidal waves, linear wave theory may be applied for an estimation of the wave mass flux and wave radiation stress, following the original concept suggested by Longuet-Higgins and Stewart (1964). In a random wave field, two typical means for the estimation are found in current practice (e.g. Dean and Dalrymple, 1991; Holthuijsen, 2007). A numerical integration may be performed on a full surface wave energy spectrum obtained via measurement or parametrization. This method accounts for incremental contributions from all individual waves considering their frequency-dependent magnitudes and kinematics. The other simpler means to approximate the parameters is often referred to as a representative wave approach in which the estimation of the parameters is based solely on some nominal waves under an assumption of a narrow-banded wave field.

Improvements in the estimation of the wave radiation stress and the wave mass flux are found in the literature, most of which are achieved by use of extended wave theory for describing the wave

* Corresponding author.
E-mail addresses: chatchawin.s@psu.ac.th (C. Srisuwan), payom.r@psu.ac.th (P. Rattanamanee), winyu@siit.tu.ac.th (W. Rattanapitikon).

http://dx.doi.org/10.1016/j.oceaneng.2016.12.024
Received 2 July 2016; Received in revised form 1 December 2016; Accepted 21 December 2016
Available online 07 February 2017

Nomenclature

$S_{\alpha\beta}$	wave-radiation stress in α and β components	FL^{-1}
h	mean water depth	L
h_o	still water depth	L
$\bar{\eta}$	wave setup level	L
u_w	wave-induced water particle velocities	LT^{-1}
η	instantaneous water surface level	L
M_α	wave-induced mass flux in α component	MT
S_{xx}	wave-radiation stress in normal x direction	FL^{-1}
M_x	wave-induced mass flux in x direction	MT
E	directional surface wave energy spectrum	L^2T
C	wave celerity	LT^{-1}
C_g	wave group celerity	LT^{-1}
f	wave frequency	T^{-1}
H	surface wave height	L
H_{rms}	root-mean-square height of random waves	L
F_η	nondirectional surface wave energy spectrum	L^2T
D	directional spreading function of wave spectrum	[-]
ϑ	coefficient in parametrized wave spectrum	[-]
f_p	peak wave frequency	T^{-1}
γ^δ	peak enhancement factor in JONSWAP spectrum	[-]
ϕ_k	depth-dependency factor in TMA spectrum	[-]
k	wave number	L^{-1}
k_p	wave number evaluated at peak wave frequency	L^{-1}
f_L	low frequency cutoff	T^{-1}
f_H	high frequency cutoff	T^{-1}
ω	wave angular frequency	T^{-1}
θ	incident wave angle	[-]
u	nondimensional parameter equal to $(\omega^2 h)/g$	[-]
u_L	nondimensional parameter u evaluated at f_L	[-]
u_H	nondimensional parameter u evaluated at f_H	[-]
L	wave length	L
L_o	deep-water wave length	L
R^2	coefficient of determination	[-]
Err.	error in estimation as percentage of mean measured value	%
Std.	standard deviation of Err. as percentage of mean measured value	%
RMSD	root-mean-square deviation as percentage of mean measured value	%
BIAS	slope of a linear line fitted through comparison between two datasets	[-]

quantities and their variations. For inside and outside of the surf zone on gently sloping beaches, Stive and Wind (1982) applied two nonlinear wave theories to determine the radiation stress and wave setup and showed that they both are qualitatively superior to the linear wave theory. Wang et al. (2008) introduced new expressions of the wave radiation stress and volume flux, reformulated by including up to the sixth-order description of surface waves. The new formulas were incorporated in a circulation model which was tested against sinusoidal waves in intermediate to deep water depths. The formulas were able to produce an accurate estimation for wave setup and setdown with, however, a very marginal improvement on the velocity profile of wave-induced currents.

More practical improvements in the subject area have been focused on estimating the parameters for a group of random waves. Such efforts are partly motivated by the fact that a narrow-band representation of the waves may cause the resulting parameters to deviate significantly from their actual quantities in the sea (Tayfun, 1986). In this type of study, the parameters obtained via a full numerical integration of the random wave spectra are typically treated as the factual best estimates, to which the estimation results yielded by any other techniques are compared and evaluated. Feddersen (2004) attempted to investigate the validity of the narrow-band approximation on a set of locally-generated waves under intermediate to deep water conditions with a wide range of wave steepness. The study showed that the approximation could lead to around 35% overestimation in the radiation stress. The selection of waves to serve as the representative parameters alone could lead to much inconsistency in the estimation.

In the present study, two novel formulas are derived and introduced for the estimation of the total wave mass flux and wave radiation stress in the normal direction. While appearing in closed form and ready for analytical applications, the new formulas offer enhanced estimation accuracies, surpassing those allowed by the representative wave approach. The derivation of the formulas starts in the next section after a brief review of related wave theory. The new solutions are then verified against synthetic time series of random waves and their best application ranges are disclosed. Various sets of field wave data are employed in a further validation, including a sensitivity analysis, in order to ensure the enhancement in the estimation capabilities. Conclusions of the study are finally made to summarize the underlying bases and practical utilities of the new formulas.

2. Estimation of wave radiation stress and wave mass flux

The underlying physics of the wave radiation stress and wave mass flux will be described here along with a review of existing techniques for estimating the parameters. The new formulas will be compared to these typical techniques later on.

2.1. Spectral-based and narrow-banded approximations

A definition sketch is given in Fig. 1 for important wave parameters that contribute to the momentum and mass fluxes under a progressive wave of height H propagating over a mean water depth h. The radiation stress is defined as the excess flow of momentum due to the presence of the wave (Longuet-Higgins and Stewart, 1964). The term can be derived using a momentum balance equation, and is fully expressed as

$$S_{\alpha\beta} = \overline{\int_{-h_o}^{\eta} [\rho u_{w\alpha} u_{w\beta} + \delta_{\alpha\beta} P]\, dz} - \delta_{\alpha\beta}\left[\frac{1}{2}\rho g \overline{\eta^2}\right] \tag{1}$$

with $S_{\alpha\beta}$ being the 2nd order tensor of the radiation stress in the horizontal directions α and β. The factor u_w indicates the fluid particle velocity induced by the wave; P is the combined dynamic and hydrostatic pressure; and δ is the Kronecker delta. The coordinate and other referencing symbols, including η, $\bar{\eta}$, and h_o, are as defined in Fig. 1. Similarly, the wave mass flux is defined as the rate of fluid mass flow passing through the vertical plane, given as follows:

$$M_\alpha = \overline{\int_{-h_o}^{\eta} [\rho u_{w\alpha}]\, dz} \tag{2}$$

in which M_α is a per-unit-width mass flux directed in the α direction. In

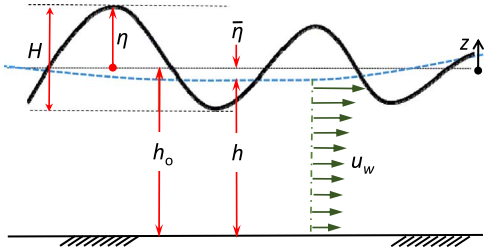

Fig. 1. Definition sketch of wave parameters associated with momentum and mass fluxes through a vertical plane.

both Eqs. (1) and (2), the integrals and the overbars indicate an upright integration over the water depth, and a time averaging over the wave period, respectively. The resulting parameters $S_{\alpha\beta}$ and M_α are therefore represented in terms of depth-integrated, phase-averaged quantities.

A common method in evaluating the above equations is to rely on linear wave theory for the description of the associated wave parameters. In respect to the actual wave field, the elements of the parameters are dependent on the alignment of the coordinate in a domain, but normally the $x-$ and the $y-$ axes are defined along the cross-shore and the longshore directions, in that order. The primary focus here will be on the normal wave radiation stress and the wave mass flux in the cross-shore direction, i.e. S_{xx} and M_x. As the waves propagate towards the shoreline, these components are usually more dynamic than those in the transverse direction (DeVriend et al., 1993). The values of S_{xx} and M_x can be computed by summing the contributions from all individual waves of all frequencies (f) and directions (θ) following

$$S_{xx} = \int_0^\infty \int_0^{2\pi} E(f,\theta)\left[\frac{C_g(f)}{C(f)}(\cos^2(\theta)+1)-\frac{1}{2}\right] d\theta\, df \tag{3}$$

and

$$M_x = \int_0^\infty \int_0^{2\pi} \left[\frac{E(f,\theta)}{C(f)}\cos(\theta)\right] d\theta df \tag{4}$$

where E is the directional surface wave energy spectrum; C and C_g are the frequency-dependent wave celerity and wave group celerity, in that order. A precise description of these celerity terms needs to consider absolute phase speeds of the waves that are propagating along with a non-zero component of a mean current. This consideration may be neglected if the intrinsic wave celerity is of a higher order of magnitude than the current, with exceptions for cases of shallow surf zones or inlets which could experience extraordinary strong mean flows.

The evaluation results in Eqs. (3) and (4) may be referred to as spectral estimates of S_{xx} and M_x which are interpreted in terms of the available wave energy and the wave celerities. In most wave measurements, they are usually taken as measured results since a direct quantification of the actual mass and momentum fluxes is not practically feasible. Now if the energy spectrum is assumed to be narrow-banded in both frequency and direction, the expressions may be simplified for the approximations of the wave radiation stress and the wave mass flux that follow (e.g. Feddersen, 2004):

$$S_{xx}^{nb} = \frac{1}{8}\rho g H_{rms}^2\left[\frac{C_g}{C}(\cos^2(\bar{\theta})+1)-\frac{1}{2}\right] \tag{5}$$

$$M_x^{nb} = \frac{1}{8}\frac{\rho g H_{rms}^2}{C}\cos\bar{\theta} \tag{6}$$

in which H_{rms} is the root-mean-square wave height; $\bar{\theta}$ is the mean energy-weighted direction of the waves; and the superscript "nb" denotes the assumption of a narrow-banded wave field. The wave celerity C and the group celerity C_g here may be evaluated at the peak (T_p) or the mean (T_m) period of the random waves. The peak period T_p is commonly applied in practice since it could readily be related to the speed of the wind that induces the wave field (e.g. Work and Srisuwan, 2010). The formulas shown in Eqs. (5) and (6) appear in analytical closed form but are based only on some representative wave parameters of the entire wave field.

2.2. Parameterized wave spectra

In the full spectral-based means of estimation, accurate information on the wave energy spectra is required, which might be achieved by use of many advanced wave measurement techniques (e.g. Young, 1994; Hoitink et al., 2007; Work, 2008). Yet, such an estimation option will always be constrained by the cost and time required for launching a wave measurement scheme, considering the immense size of the coastal ocean alone. When reliable information on regional wave climates is available, an alternative provision of the required spectral wave data and independent estimates of wave parameters may be attained via parameterization of wave spectra.

In the spectral estimates of wave radiation stress and wave mass flux in Eqs. (3) and (4), the surface wave energy spectrum E may be rewritten to consist of two parts that follow:

$$E(f,\theta) = F_\eta(f)D(f,\theta) \tag{7}$$

where F_η is the non-directional energy spectrum, and D is the directional spreading function of the waves. Based on numerous sets of historical wave spectra, Pierson and Moskowitz (1964) suggested that the energy spectrum F_η of fully-developed surface waves in deep water should follow the well-known Pierson-Moskowitz (PM) spectrum, given as

$$F_\eta^{PM}(f) = \vartheta g^2(2\pi)^{-4}f^{-5}\exp\left[-\frac{5}{4}\left(\frac{f}{f_p}\right)^{-4}\right] \tag{8}$$

in which f_p is the peak wave frequency, and ϑ is an empirical coefficient. Two major modifications were applied to the PM spectrum since its first introduction. The fetch and duration limits of wave generation were taken into account, which led to the JONSWAP wave spectrum (Hasselman et al., 1973). The other addition was to account for the effect of finite water depth on the wave field (Bouws et al., 1985), resulting in what is known today as the TMA wave spectrum that follows:

$$F_\eta^{TMA}(f) = F_\eta^{PM}\,\gamma^\delta\,\phi_k \tag{9}$$

in which γ^δ is the peak enhancement factor which accounts for the limitations of fetch and duration imposed in the JONSWAP spectrum. The water depth dependency factor ϕ_k that generates the TMA spectrum can be written as

$$\phi_k(f,h) = \left[k(f,h)^{-3}\frac{\partial k(f,h)}{\partial f}\right]\Big/\left[k(f,\infty)^{-3}\frac{\partial k(f,\infty)}{\partial f}\right] \tag{10}$$

where h and k indicate the water depth and the wave number, respectively. Likewise, the directional spreading of the waves $D(f,\theta)$ in Eq. (7) may also be characterized through a parametric relationship, for example, using a cosine-squared function (Hughes, 1985). Once completed, a parameterized wave spectrum may readily be applied in the estimation of the wave radiation stress and the wave mass flux. This technique helps to eliminate the need for a field measurement of wave spectra mentioned earlier.

3. New analytical formulas

The previous section shows that two general options for the estimation of S_{xx} and M_x are the spectral-based numerical integration and the representative wave approach. Optionally, the former may incorporate the use of parameterized wave spectra, but in either case, the numerical scheme involved does not allow a closed-form solution for the problem. Here, a new set of closed-form, spectral-based analytical solutions will be developed for the estimation purpose.

3.1. Formulation of solutions

The proposed solutions will be formulated based primarily on physical asymptotes and calculus of the linear wave theory. This first introduction of the solutions will be focused on non-directional quantities of the target wave parameters, which can be a normal radiation stress in a uni-directional wave field or a total mass flux of random waves. The formulation may start from the spectral estimates expressed earlier in Eqs. (3) and (4), which can be rewritten respec-

tively for the wave radiation stress and the wave mass flux under the given condition as

$$S_{xx} = \int_{f_L}^{f_H} F_\eta(f)\left[\frac{2C_g(f)}{C(f)} - \frac{1}{2}\right] df \tag{11}$$

and

$$M_x = \int_{f_L}^{f_H} F_\eta(f)/C(f)\, df \tag{12}$$

where f_L and f_H are the lower bound and the upper bound of the frequency range of interest. Note that the wave energy is now represented via the non-directional spectrum F_η only, according to the conservation of energy in the wave field such that $\int_0^{2\pi} D(f, \theta)\, d\theta = 1$.

An appropriate choice of the parameterized energy spectrum F_η may be selected for the characteristics of a target site. Here, a fully-developed sea in arbitrary water depths is considered with its surface wave energy that distributes following:

$$F_\eta(f) = \vartheta g^2 (2\pi)^{-4} f^{-5} \exp\left(-\frac{5}{4}\left(\frac{f}{f_p}\right)^{-4}\right).\ \phi_k(f, h) \tag{13}$$

where the multiplier ϕ_k is the depth-dependency factor which approaches unity in deep water conditions. Meanwhile, the factor causes the energy to decrease across the spectrum due to the effect of finite water depth. In this equation, the peak enhancement γ^δ, which appears earlier in Eq. (9), is dropped out because it is equal to unity for a fully-developed sea.

In an attempt to arrive at a complete set of analytical solutions, the terms in Eqs. (11) and (12) must be first rearranged into integrable forms. This can be achieved by use of linear wave theory in which the dispersion relation of waves in a finite water depth is given as

$$k = \frac{\omega^2}{g \tanh(kh)} \tag{14}$$

where ω is the angular frequency of the wave ($\omega = 2\pi f$). This relationship can be substituted into the expression of the depth-dependency factor $\phi_k(f, h)$, given previously in Eq. (10), to allow its new form that follows:

$$\phi_k(f, h) = \left(\frac{\omega^5}{2\, g^2}\right)\left(k^{-3}\frac{\partial k}{\partial \omega}\right) \tag{15}$$

which may still not be evaluated directly since the wave number k in the dispersion relation is not in an explicit form. A possible solution is to substitute an alternative form of k into Eq. (15) using an approximate relation suggested by Eckart (1952), given as

$$k = \frac{u}{h\sqrt{\tanh u}} \tag{16}$$

in which u is a non-dimensional factor equal to $(\omega^2\, h)/g$. Possible errors in the use of this approximation are dependent on the relative water depth (kh), but they will be limited to a maximum of 5% according to an investigation conducted later on (see Fig. 3). Using this alternative expression of k, the derivative term in Eq. (15) can be executed and manipulated to yield

$$\phi_k(f, h) = \tanh(u) + \frac{u}{2}[\tanh^2(u) - 1] \tag{17}$$

This expression can be inserted into Eqs. (11) and (12) which would thus be ready for evaluation. Note that explicit forms of the wave celerity factors in the same equations can also be obtained by use of Eckart's dispersion relation, obeying $C = \omega/k$ and $C_g = d\omega/dk$, where ω is the angular wave frequency and k is the wave number. The effect of mean current is excluded here and it will be shown later to be not significant in the application range of the new formulas. By transforming the integration variable f into the non-dimensional factor u, the two principal equations can be rewritten as

$$S_{xx} = A_s\left[\int_{u_L}^{u_H} u^{-3}e^{-Bu^{-2}}\left(\tanh(u) + \frac{u}{2}[\tanh^2(u)]\right) du - \int_{u_L}^{u_H} u^{-3}e^{-Bu^{-2}}\, du\right] \tag{18}$$

and

$$M_x = A_m \int_{u_L}^{u_H} u^{-5/2}e^{-Bu^{-2}}\left(\frac{\tanh(u) + \frac{u}{2}[\tanh^2(u) - 1]}{\sqrt{\tanh(u)}}\right) du \tag{19}$$

with the groups of known constants:

$$A_S = \frac{\vartheta h^2}{4\pi};\quad A_M = \frac{\vartheta h^{3/2}}{2\, g^{1/2}};\quad \text{and}\quad B = \frac{5\, h^2}{4\omega_p^{-4} g^2} \tag{20}$$

in which the peak angular wave frequency $\omega_p = 2\pi f_p$, and the integral limits u_L and u_H are the values of u corresponding to the low and the high frequency cutoffs in the wave spectrum. Noticeably, Eqs. (18) and (19) may be arranged in many other forms but they are kept in these formats for practical reasons which will be shown next.

3.2. Evaluation of analytical expressions

For the wave radiation stress S_{xx}, the two integral terms in Eq. (18) must be evaluated over the given interval to obtain a closed-form solution. The complexity that exists in the first integral, due to the co-existence of the power, the exponential, and the hyperbolic tangent terms (tanh), is first resolved by use of replacement functions obtained from an asymptotic analysis. For the tanh term in Eq. (18), the analysis over a wide range of the non-dimensional factor $u = (\omega^2\, h)/g$ can clearly show that

$$\tanh(u) + \frac{u}{2}[\tanh^2(u)] \approx u, \quad \text{for} \quad 0 < u \le u_* \tag{21}$$

and

$$\tanh(u) + \frac{u}{2}[\tanh^2(u)] \approx \frac{u}{2} + 1, \quad \text{for} \quad u > u_* \tag{22}$$

where the threshold factor u_* is simply equal to 2.0 in this case. For clarity, a comparison between the exact values and the values allowed by these replacement functions is given in Fig. 2a. With these asymptotes and function limits, the first integral in Eq. (18) may be separated again into three sub-integration terms which lead to:

$$S_{xx} = A_s\left[\int_{u_L}^{u_*} (u^{-2} + u^{-3})e^{-Bu^{-2}}\, du + \frac{1}{2}\int_{u_*}^{u_H} u^{-2}e^{-Bu^{-2}}\, du\right] \tag{23}$$

These new terms can thus be prepared for an integration by parts and by substitution together with aids of the non-elementary Gauss error function (erf) that is defined in an integral form as

$$\mathrm{erf}(Z) = \frac{2}{\pi}\int_0^Z e^{-t^2} dt \tag{24}$$

which subsequently allows an evaluation of Eq. (23) to yield

$$S_{xx} = \frac{A_s}{4}\sqrt{\frac{\pi}{B}}\left[\mathrm{erf}\left(\frac{\sqrt{B}}{u_L}\right) - \mathrm{erf}\left(\frac{\sqrt{B}}{u_*}\right)\right] + \frac{A_s}{2B}[e^{-(B/u_H^2)} - e^{-(B/u_*^2)}] \tag{25}$$

which is the final closed-form, analytical solution for the estimation of the wave radiation stress S_{xx} in a random wave field.

A similar approach can be applied to the integral expression of the wave mass flux given earlier in Eq. (17). Over a wide range of the non-dimensional factor u, the values of the tanh term associated with the expression are found to approach certain asymptotes:

$$\frac{\tanh(u) + \frac{u}{2}[\tanh^2(u) - 1]}{\sqrt{\tanh(u)}} \approx \frac{u}{2}, \quad \text{for} \quad 0 < u \le u_* \tag{26}$$

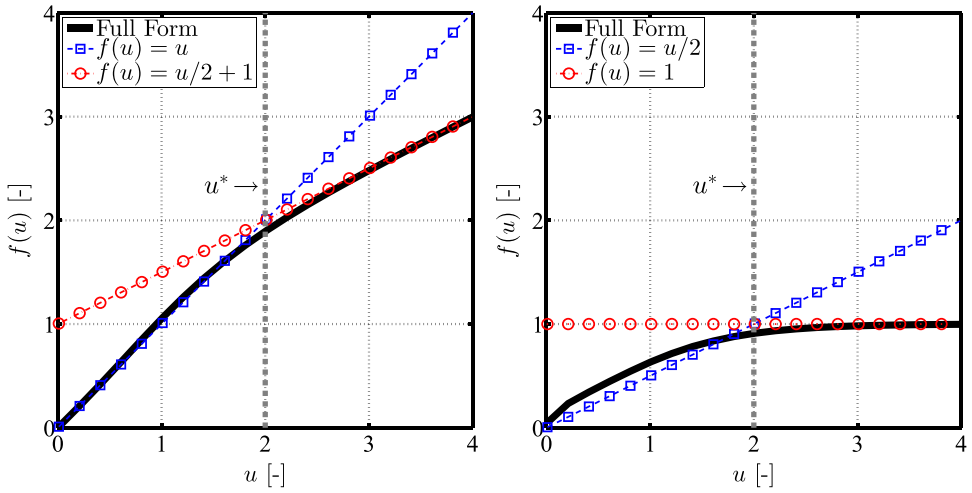

(a) For S_{xx} **(b)** For M_x

Fig. 2. Exact values of tanh terms compared to values yielded by asymptotic functions utilized in the derivation of the new formulas. Note that the value of $u = u^*$ indicates the change of the asymptotic functions. (a) For S_{xx} (b) For M_x.

and

$$\frac{\tanh(u) + \frac{u}{2}[\tanh^2(u) - 1]}{\sqrt{\tanh(u)}} \approx 1, \quad \text{for} \quad u > u_* \tag{27}$$

in which the threshold factor u_* is still equal to 2.0. The results from this asymptotic analysis are shown in Fig. 2b for clarity. Using the replacement functions, Eq. (19) can be rewritten in a new form that follows:

$$M_x = A_m\left[\frac{1}{2}\int_{u_L}^{u_*} u^{-3/2}e^{-Bu^{-2}}\,du + \int_{u_*}^{u_H} u^{-5/2}e^{-Bu^{-2}}\,du\right] \tag{28}$$

Once rearranged for integration by parts and by substitution, Eq. (28) can be evaluated to yield a final closed-form, analytical solution for the estimation of the total wave mass flux in a random wave field:

$$M_x = \frac{A_m}{4B^{1/4}}\left[i\Gamma\left(\frac{1}{4}, \frac{B}{u_L^2}\right) - i\Gamma\left(\frac{1}{4}, \frac{B}{u_*^2}\right)\right] + \frac{A_m}{2B^{3/4}}\left[i\Gamma\left(\frac{3}{4}, \frac{B}{u_*^2}\right) - i\Gamma\left(\frac{3}{4}, \frac{B}{u_H^2}\right)\right] \tag{29}$$

where $i\Gamma$ is an incomplete gamma function defined such that

$$i\Gamma(\lambda, Z) = \int_0^Z e^{-t}\,t^{(\lambda-1)}dt \tag{30}$$

which represents a definite integral of the gamma function spanning from 0 to the variable limit Z. Due to this original lower bound at zero, each of the two terms in Eq. (29) includes a pair of incomplete gamma expressions for an evaluation between non-zero variable limits, e.g. from u_L to u_* in the first term.

Eqs. (25) and (29) are the new analytical formulas introduced here for the estimation of non-directional, total amounts of the normal wave radiation stress (S_{xx}) and the wave mass flux (M_x). Their derivations were based on the assumption of a fully-developed sea of random waves, of which the energy components and associated kinematics are described by linear wave theory. The formulas will be executable in any computing environments in which the error and the gamma functions are built-in routines. This simple requirement should be satisfied in most scientific computing devices and spreadsheet programs. In the next section, the new formulas will be investigated for their behaviors, focusing on validity in the problem formulation and the derivation accomplished here.

3.3. Investigation on development of new formulas

The development of the new formulas introduced in Eqs. (25) and (29) involves several assumptions and approximations which will be verified in this section.

The use of Eckart's solution in Eq. (16), in lieu of the exact dispersion relation in Eq. (14), needs to be first investigated. Note that this approximation is applied in the evaluations of the depth-dependency factor ϕ_k and the kinematic factors including the wave celerity C and the wave group celerity C_g. In Fig. 3, values of the wave numbers k yielded by these expressions are compared in terms of the non-dimensional wave length L/L_o. For the values of kh between $\pi/10$ to π, corresponding to a transitional water depth, the error involved with the approximation is found to be non-zero, but features a very small maximum of around 5%. The magnitude of the error tends to diminish in the lower and upper bounds of kh. Initially, this tendency suggests that the misestimation that could arise due to the use of the approximate dispersion relation should be minimal.

The use of asymptotic relations of the hyperbolic tangent terms (tanh) in Eqs. (21) and (22), and Eqs. (26) and (27) also needs to be investigated. In Fig. 2a and b shown previously, the resulting values of the terms from the asymptotes and the exact tanh functions are compared for the expressions of S_{xx} and M_x, respectively. Here, the deviations found in the comparison are illustrated quantitatively in Fig. 4 which shows that the asymptotes adopted in the formulation of S_{xx} is found to be associated with less than 5% in approximation errors. For the asymptotic form for M_x, the possible errors may rise to

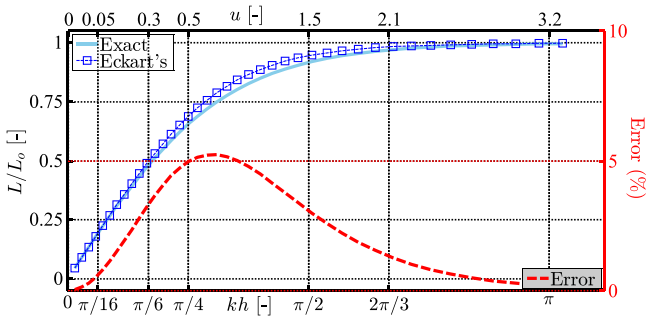

Fig. 3. Deviations found in the comparisons between exact and approximate terms of the dispersion relation. Percent error (Δ) is shown with respect to the right axis. The results are given respect to the relative depth kh and the non-dimensional factor u shown on the bottom and the top horizontal axes, respectively.

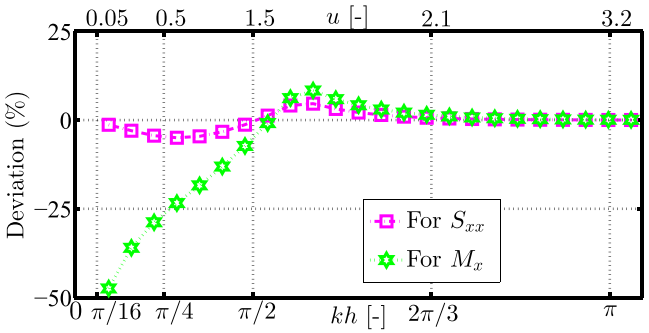

Fig. 4. Deviations found in the comparisons between exact tanh terms and asymptotic functions utilized in the derivation of the new formulas. The results are computed based on the values illustrated in Fig. 2.

50%, but such a high percentage is only found in a low range of the non-dimensional parameter ($u < 0.5$) where the base values from the exact tanh term are very small.

The investigations here may indicate that the biases involved with individual terms in the development of the new formulas should be limited. Nevertheless, the eventual impact may still not be concluded for the new formulas regarding their accuracy and precision, defined as the closeness of the estimates to exact values and the proximity of the estimates, respectively. These two indicators will be dependent on both water depth and wave frequencies, and could also vary due to both underestimation and overestimation. The only means to reach a conclusion would be to test the complete forms of the new formulas against spectral wave data which is illustrated in the next section.

4. Verification and validation of the new analytical formulas

The newly developed formulas are validated and verified here using three separate sets of spectral wave data. Their accuracy and precision are evaluated based on the best possible estimates from the surface wave measurements available, except in the synthetic test with known theoretical values of the interested parameters. The major objective in each of the tests and the results found in the analyses are discussed below.

4.1. Synthetic wave data

The primary goal in this section is to find acceptable conditions in which the new analytical formulas could be applied. The use of synthetic wave spectra would suit this need since the control parameters and the wave conditions can be specified in the test. To obtain the proposed synthetic data, parameterized wave spectra were first constructed assuming fully-developed seas and arbitrary water depths, following the TMA spectral form given earlier in Eq. (9). Surface time series of the waves were then simulated, using a random phase method in which irregularity of the wave field is included. A total of 300,000 realizations, with different peak wave frequencies (f_p) and water depths (h), were generated and transformed into the final wave spectra for use in the test. Nominal wave parameters employed in the representative wave approach for comparison purpose, including H_{rms} and T_p, were computed based on moments of the energy spectra.

Of many physical conditions, the relative water depth (kh) appears to be most critical to the accuracies of the new analytical formulas. This influence arises according to several derivation techniques adopted in the solution methods, as discussed in the previous section. In a random wave field, the dominant wave at the peak wave frequency f_p and wave number k_p may be used to define a proximal relative water depth k_ph. Over a wide range of this factor, Fig. 5 illustrates percent occurrences of the computed errors in the tests for S_{xx} and M_x. The errors are defined according to the differences between the estimated results, from the representative wave approach and the new analytical solutions, and the exact values yielded by the full numerical integration. The percent occurrences are based on synthetic spectra that fall into each of the given ranges of k_ph, of which the percentage from the total 300,000 synthesized data is also shown in the figure.

In the lower range of $k_ph < \pi/3$ in Fig. 5a, very high percent occurrences are shown to accumulate around the negative percent errors of 50% which imply that the new solutions tend to underestimate most values of the radiation stress S_{xx} by half their exact values. The representative wave approach, meanwhile, is found to be associated with around 25% overestimation of the parameter. The two techniques are found to allow more accurate estimates as the value of k_ph increases. It is in the range of $3\pi/4 < k_ph < 5\pi/4$ that the new analytical solution appears to outperform the traditional approach. Beyond this range, both of the techniques appear to perform considerably well since all of the estimates are within ±10% errors. Throughout the evaluation in Fig. 5, much narrower distributions of the percent occurrences over the errors are always found in the use of the new solution, suggesting that its estimation precision may also be another positive aspect, besides the accuracy.

In the estimation of M_x, Fig. 5b shows that in the lower range of $k_ph < \pi/3$, both of the techniques tend to underestimate most values of the parameter by −10 to −20%. The performance of the new formula then appears to enhance as the range of k_ph increases towards the deep water limit. An opposite change is found in the estimates yielded by the representative wave approach, as the underestimation arises to −15 to −25%. A narrower distribution of the computed results may be found here in the use of the representative wave technique, but such superior precision seems to decay quickly with the accuracy in higher ranges of k_ph.

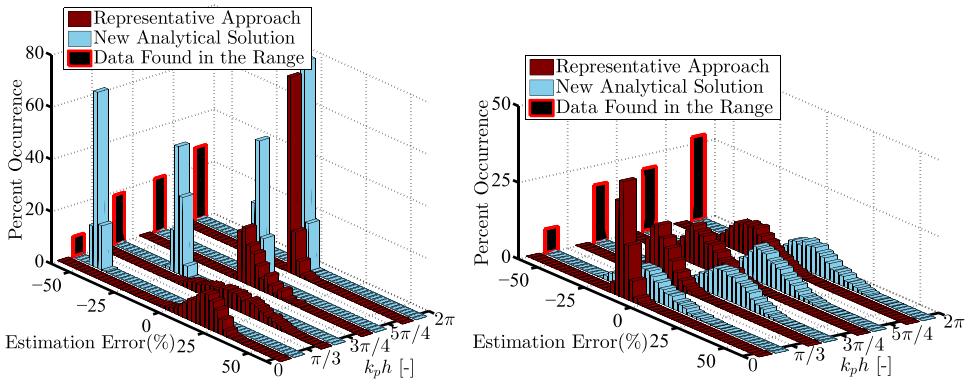

(a) For wave radiation stress S_{xx} **(b)** For wave mass flux M_x

Fig. 5. Percent occurrences of estimation errors yielded by the new solutions and the representative wave approach. The results are given for four ranges of the relative water depth k_ph. The percentage of the total 300,000 synthetic data that falls into each range of k_ph is also shown on the left of the figures. (a) For wave radiation stress S_{xx} (b) For wave mass flux M_x.

The above findings may confirm that in both of the estimations for S_{xx} and M_x, the new solutions will become a superior option to the representative wave approach under some higher ranges of k_ph. To account for both the accuracies and the precisions, certain applicable ranges of the new formulas are justified based on the root-mean-square deviation (RMSD). This statistical factor is defined as the square root of the mean squared error between the estimated and the exact numerical values. Fig. 6 shows the values of RMSD associated with the estimates, yielded by the two different techniques. Note that the plotted lines are not perfectly smooth due to the systematic randomness in the synthetic data.

In Fig. 6a, the new formula for S_{xx} is associated with a substantial deviation in the lower range of k_ph, which was found earlier in Fig. 5a to be an underestimation. As the limit of k_ph approaches $\pi/2$, such deviations from the two different techniques become more comparable before the new solution appears to provide more accurate estimates for greater values of k_ph. The representative wave approach may regain a superior position when the relative water depth lies between $7\pi/4$ to $9\pi/4$, but the magnitude of error in such a range should be negligibly small ($< 0.5\%$). This comparison reveals that the new formula for S_{xx} should be suitable for use when the factor k_ph is greater than $\pi/2$. This threshold may be referred to as an upper intermediate water depth limit, for typical shallow-water and deep-water asymptotes defined where $kh < \pi/10$ and over $kh > \pi$, respectively (Dean and Dalrymple, 1991).

In Fig. 6b, the RMSD values yielded by the two different techniques in the estimation of M_x are compared. For $k_ph < \pi/4$, the new analytical solution has a very substantial deviation of up to 80%. This misestimation arises as a result of the simplification on the hyperbolic tangent term (tanh) that is least accurate in such a range of relative water depth (see Fig. 4). For higher values of k_ph, the new solution exhibits a superior performance to the representative wave approach, which is especially clear when the factor k_ph is greater than $\pi/2$. This clarity suggests that the applicable range of the new analytical formula for M_x should be identical to that of the new formula of S_{xx}, defined at $k_ph > \pi/2$. Within this upper intermediate to deep water environment, the mean current should be of a lower order of magnitude than the wave celerity and only leads to a minimal effect in the estimation of the parameters. It will be investigated next how the capabilities of the new formulas and the representative wave approach are compared under a practical application on field wave spectra with higher uncertainty and randomness.

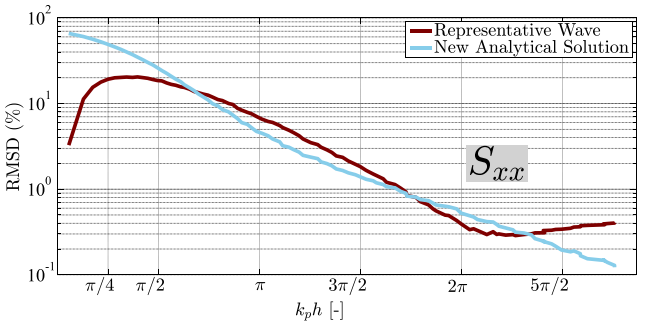

(a) For wave radiation stress S_{xx}

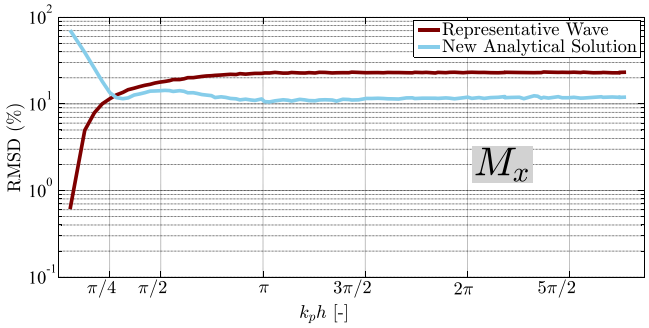

(b) For wave mass flux M_x

Fig. 6. Comparisons between the estimation errors from the new solutions and from the representative wave approach. The results are based on the 300,000 synthetic tests and are given in terms of root-mean-square deviation (RMSD) as a function of the relative water depth k_ph. (a) For wave radiation stress S_{xx} (b) For wave mass flux M_x.

4.2. Nearshore wave buoy data

The performances of the new formulas are reexamined here based on wave data from an in-situ wave measurement device. The primary objectives are to confirm the applicable ranges of the formulas defined previously as a function of k_ph, and to investigate possible sensitivities of the formulas on the variation of sea state and energy distribution in the wave field.

More than 16,000 hourly records of spectral waves achieved by Work (2008) are utilized in the validation here. Using a surface-following wave buoy, the data were collected at a site near the Savannah River entrance channel in the State of Georgia, USA. The mean water depth at the site is 13.6 m with a tidal range of 2.1 m. For a period of 2.5 months, an acoustic Doppler current profiler (ADCP) was also collocated with the buoy to verify the measured wave spectra. Besides the reliability, the spectral estimates from this work are suitable for testing the new analytical formulas because of the wide variation of their associated relative water depths (k_ph). The data sets feature both directional and non-directional wave spectra, but using only the latter is sufficient for the present validation purpose.

In the pre-processing stage, wave energy components contributed by sea and swell in the spectra were separated following the methodology outlined by Work and Srisuwan (2010). The local wind-induced waves, referred to as the sea, are utilized for the verification as the new solutions were developed based on the parameterized spectral form that describes the energy distribution of such waves. The mean water depths, which were not recorded by the buoy but are required in the new solutions, were reproduced using a tidal harmonic analyzing tool introduced by Pawlowicz et al. (2002). A part of the time series from the reproduction was verified against available hourly data from the ADCP, and the error associated was found to be within $\pm 5\%$.

Using the numerical approach, best estimates of the wave radiation stress (S_{xx}) and the wave mass flux (M_x) were computed from the measured wave spectra. These estimates were then compared to the values yielded by the new analytical solutions and the representative wave approach from which the mean absolute errors are shown for many ranges of k_ph in Fig. 7a. Note that the only coefficient in the new formulas (ϑ) was treated as an adjustable factor, which constrains the conservation of the total wave energy. This action certainly does not interfere any comparisons among the different sets of results nor their sensitivities.

For k_ph below the applicable limit at $\pi/2$, the estimation errors on S_{xx} from the two techniques are opposite, with the new analytical solution tending to underpredict the parameters. Beyond the threshold, such an underestimation decreases and the new formula appears to allow better estimates. This tendency can be confirmed in Table 1, in which the percent errors and their standard deviations are summarized. The absolute errors may be slightly lower for the representative wave approach which is, however, involved with somewhat higher standard deviations in any ranges of k_ph. The reduction in the computed errors in the representative approach also occurs as its prediction trend changes over the values of k_ph. This fact can be observed in Fig. 7a at $k_ph \approx 2\pi/3$ where the computed errors progress from an overestimation to an underestimation.

In Fig. 7b, the magnitudes of the wave mass flux (M_x) below the limit of $k_ph < \pi/4$ were found to be underestimated by both of the estimation techniques. As the value of k_ph increases beyond $\pi/2$, the negative deviation in the new solution diminishes quickly and tends to

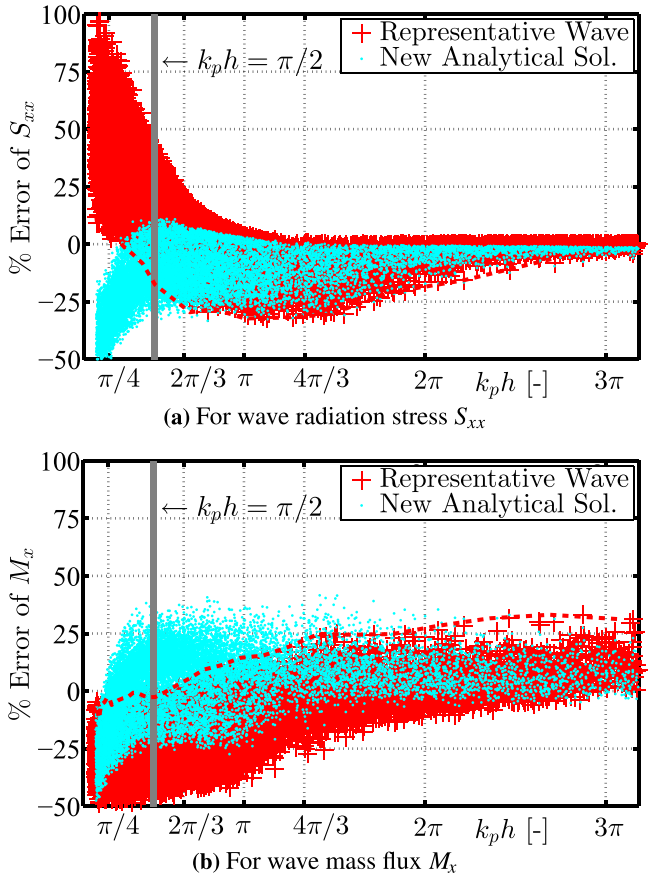

(a) For wave radiation stress S_{xx}

(b) For wave mass flux M_x

Fig. 7. Estimation errors found in the tests of the new solutions and the representative wave approach against wave buoy data. The errors associated with each technique are computed based on the exact values yielded by the full numerical integration. Dash lines indicate the underlying lower and upper bounds of the representative wave results. (a) For wave radiation stress S_{xx} (b) For wave mass flux M_x.

Table 1
Statistical factors computed for values of wave radiation stress S_{xx} yielded by the two different techniques. Note that the factors are based on the comparison with the exact numerical results. R^2 is the coefficient of determination, |Err| is the mean absolute error in percent, and Std is the standard deviation of error as percentage of the mean.

Analyzing Technique: Range, (% **occurred**)	**Representative Wave**			**New Analytical Solution**		
	R^2 [-]	|Err.| (%)	Std. (%)	R^2 [-]	|Err.| (%)	Std. (%)
$0 < k_p h \le \pi/3$, (23%)	0.75	41.79	16.11	0.62	29.37	9.24
$\pi/3 < k_p h \le \pi/2$, (20%)	0.93	25.09	13.82	0.88	15.95	9.05
$\pi/2 < k_p h \le 3\pi/4$, (22%)	0.99	9.81	11.65	0.89	12.21	9.18
$3\pi/4 < k_p h \le 3\pi/2$, (21%)	0.93	10.34	9.28	0.90	11.26	8.64
$3\pi/2 < k_p h \le 3\pi$, (11%)	0.95	4.51	5.07	0.94	5.35	4.86
$k_p h > 3\pi$, (3%)	1.00	0.49	0.70	1.00	2.51	0.72

neutralize to a mean value of zero. This improvement is also observed under the representative wave approach but appears to be a more gradual, monotonic process over the values of $k_p h$. In Table 2, the mean absolute errors from the new solution are shown to be up to 13% lower than those of the representative wave approach. In some ranges of $k_p h$, however, the standard deviations of the errors induced by the new solution are higher by 2–3%. This tendency occurs according to the fact that more neutral results from the new solution, while featuring smaller mean absolute errors, initiate a wider total range of errors as they are associated with comparable magnitudes of underestimation and overestimation as illustrated in Fig. 7b.

The new analytical solutions can be verified according to the results shown in Fig. 7. The option in choosing a wave period, e.g. T_p or T_m, will not lead to a certain improvement in the representative approach that involves both underestimation and overestimation of the wave parameters. In any case, the performances of the new solutions could also be dependent on some other factors. Therefore, three additional parameters commonly used to describe the random sea are investigated for their possible influences on the computed values of S_{xx} and M_x. One is the relative wave height, expressed simply as the ratio between the mean wave height and the water depth (H/h). This parameter behaves like an indicator for the measure of water depth, but it is classified on the basis of the wave height instead of the peak wave number adopted in the factor $k_p h$.

Another influential parameter is for the quantification of the overall steepness of the random sea, defined as the spectral steepness factor S_p that follows:

$$S_p = 2\pi \left(\frac{H_{m0}}{g T_p^2} \right) \tag{31}$$

where H_{m0} and T_p are the spectral-based significant wave height and the peak wave period, in that order. The relativity between these two physical wave parameters indicates a non-dimensional steepness of the wave field, interpreted more straightforwardly as a wave height to wave length ratio.

The other testing factor is for the measure of the relative width of the spectrum, or the degree at which the energy is distributed over the entire frequency bands. According to Longuet-Higgins (1975), this characteristic may be quantified by use of the spectral width parameter ν defined as

$$\nu = \left(\frac{M_0 M_2}{M_1^2} - 1 \right)^{1/2} \tag{32}$$

in which M_n is the nth moment of the wave energy spectrum. Typical values of ν may span between 0.3 and 0.5 in the TMA and JONSWAP parameterized wave spectra, with a similar range also found in most wind-sea dominated field wave spectra (e.g. Soares and Carvalho, 2003).

All the three hypothesized parameters were first computed for all of the available wave spectra. The errors involved in the two estimation techniques are subsequently related as functions of these influential parameters, as shown in Fig. 8. The sensitivities due to the relative wave height (H/h) are depicted in Fig. 8a and b for S_{xx} and M_x, respectively. Overall, both of the new solutions appear to be more accurate in the lower range of H/h, simply because of the fact that most smaller values of H/h are found under deeper water conditions, i.e. in analogy to possessing large values of $k_p h$. In comparison to the representative wave approach, the new solution for S_{xx} shows a clear superiority for $H/h \le 0.08$, but marginally greater errors for higher H/h. The new solution for M_x results in around 15% and 3% smaller errors for the lower and the higher ranges of H/h, respectively.

For both S_{xx} and M_x, the two estimation techniques are found to produce certain errors that form a concave-up parabola over the steepness factor S_p, as shown in Fig. 8c and d. In the upper range of S_p, the wave spectra tend to be negatively-skewed with much of their energies in higher frequencies. The errors found at this limit of S_p are thus relatively high since such irregular spectral forms are neither narrow-banded nor resembling the form of wind-induced waves. For smaller values of S_p, the new formulas appear to be the better option since the wave spectra become more similar to that of their base parameterized spectrum, but they are still not narrow-banded. The new formulas are also able to produce more accurate results than the

Table 2
Statistical factors computed for values of wave mass flux M_x yielded by the two different techniques. See Table 1 for details.

Analyzing Technique:	**Representative Wave**			**New Analytical Solution**		
Range, (% occurred)	R^2 [-]	|Err.| (%)	Std. (%)	R^2 [-]	|Err.| (%)	Std. (%)
$0 < k_p h \leq \pi/3$, (23%)	0.61	26.73	8.60	0.91	15.00	12.26
$\pi/3 < k_p h \leq \pi/2$, (20%)	0.84	24.34	8.68	0.98	10.79	12.13
$\pi/2 < k_p h \leq 3\pi/4$, (22%)	0.92	19.53	9.34	0.94	13.71	12.48
$3\pi/4 < k_p h \leq 3\pi/2$, (21%)	0.97	12.60	11.01	0.94	12.82	12.26
$3\pi/2 < k_p h \leq 3\pi$, (11%)	0.98	6.41	7.92	0.94	9.14	7.86
$k_p h > 3\pi$, (3%)	0.93	16.41	8.60	0.97	6.89	6.57

representative wave approach according to the cross-spectrum integration that better reflects irregularity in the wave field. Since this superiority is confirmed in the majority of the tests, the steepness factor S_P should not be a critical indicator for selection of the estimation techniques.

The sensitivities of the two techniques on the relative width of wave spectra ν are investigated in Fig. 8e and f, for the estimations of S_{xx} and M_x, respectively. In both cases, the estimation errors are clearly found to rise as the values of ν increases. This is a scenario when the energy spectrum of the wave field has a wider frequency bandwidth, thus violating the narrow-banded assumption and deviating somewhat from the parameterized wave spectrum. The analysis shows that the new analytical solution for M_x outperforms the representative approach for the entire range of ν. Meanwhile, the new analytical solution for S_{xx} appears to be the superior option for values of ν between 0.27 and 0.54, agreeing with the fact that this typical range found in the parameterized wave spectrum is the basis for the development of the new formulas.

The performances of both of the estimation techniques seem to decline for a very high range of ν. For values of ν beyond 0.54, the representative approach may appear to provide the better estimates of S_{xx}, but in fact, neither of the techniques should be employed because their underlying assumptions are already violated. The spectra are not narrow-banded, nor can they be formed via the parameterization. This extreme condition, however, is generally rare in wind-induced surface wave spectra and, as illustrated in Fig. 8e and f, less than 2% of the wave spectra tested here fall into such a scenario.

Several conclusions can be drawn from the above verification. The applicable ranges of the new solutions, previously defined using synthetic data for the relative water depth $k_p h \geq \pi/2$, can be confirmed once again under the tests with these reliable measured wave spectra. The new formulas may seem to be somewhat sensitive to the relative spectral wave height (H/h) and the sea steepness (S_P), but these factors are found to be closely relative to $k_P h$. The spectral shape that favors the use of the new solutions should follow that of their prototype parameterized wave spectrum, which may be indicated by the spectral width factor ν. In any case, if the tested sensitivity factors H/h, S_P, and ν are within typical ranges of wind-induced waves (e.g. Soares and Carvalho, 2003), they should lead to marginal effects in the estimation. With this major reason, the new formulas will next be tested in a practical application with a major concern on the relative water depth $k_P h$ that is the most influential factor.

4.3. NOAA wave buoy data

To reassure their performances under various field conditions, the new analytical formulas are verified again based on field wave energy spectra available at nine locations along the US Atlantic Coast and the Gulf of Mexico. This spectral wave information is obtained from a network of data collecting buoys developed and operated by the National Data Buoy Center (NDBC) of the US National Oceanic and Atmospheric Administration (NOAA). Details of the measurement stations can be found in Table 3. A total of 7,000 hourly spectral wave records from each site were utilized in the verification. The raw data were preprocessed following the same techniques applied in the previous section, except for the hourly tidal variations, which should be negligible relative to the local mean water depths which range from 19.5 to 82.2 m.

The best estimates of S_{xx} and M_x yielded by the exact numerical integration were treated as a benchmark for the evaluation of the representative wave approach and the new analytical formulas. For clarity, the estimation results may be classified into two separate groups. One includes those from Stations 1 to 5 which also see a lower intermediate water depth ($k_p h < \pi/2$), while the other is from Stations 6 to 9 with an upper intermediate water depth and beyond. In Fig. 9a and b, the results from the first group with shallower water waves show that the values of S_{xx} from the new solutions tend to be slightly underestimated, but the opposite trend is found for those from the representative wave approach. Each estimation bias may be clearly observed based on the linear line fitted through the comparison, noting that the line must feature a one-to-one slope without any bias.

A careful consideration of Fig. 9a and b can reveal that the new solution allows estimation results of S_{xx} that are associated with substantially smaller absolute errors and scatter. To ensure these facts, three quantitative factors based on the results from the two techniques are inter-compared, including the mean absolute error, the estimation bias, and the standard deviation of the errors given as a percentage of the mean. Residuals of all these factors from the intercomparison, taking the new solution results as minuends, are summarized in Table 4. All of these residuals, featuring negative values in the estimation of S_{xx} for Stations 1–5, can confirm the superiority of the new analytical solution over the representative wave approach.

A similar comparison is performed based on the data from the deeper group of stations (Nos. 6–9), with two sets of results illustrated in Fig. 9c and d. In these cases, both estimation techniques seem to allow very accurate results, but the new analytical solution still appears to be a superior option in terms of estimation precision. This tendency can be confirmed based on the analysis in Table 4, which reveals that the standard deviations of the estimates can be up to 7% higher for the representative wave approach. This number implies an increased chance in encountering a substantial error in any trial of the representative solution. A common scenario for this case is when the characteristics of the sea discourage the narrow-banded assumption, thus disallowing the use of any nominal wave for a precise description of the wave field.

The resulting estimates of the wave mass flux (M_x) are illustrated in Fig. 10a and b for two cases from the first group of data sets. The results clearly show that the representative wave approach tends to underestimate the results while the new analytical solution is associated with an overestimation. The former tendency appears be somewhat more significant and can be confirmed in Table 4 to lead to up to a 20% higher bias than the possible overestimation in the new solution. The estimation accuracy may also be compared more directly using the mean absolute errors, reported to be around 7–10% smaller in the use of the new analytical formula. The resulting standard deviations of the

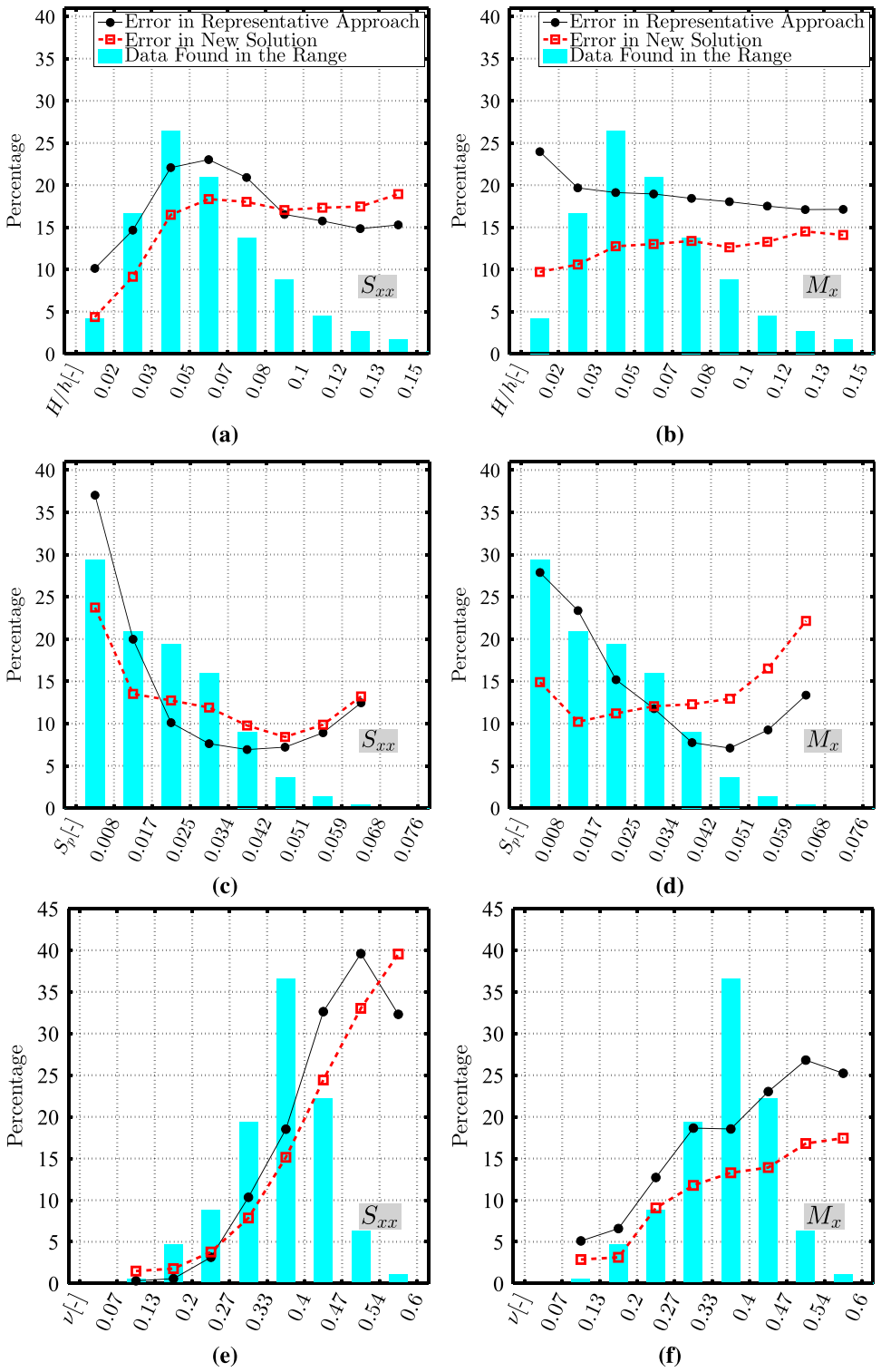

Fig. 8. Variation of the estimation errors found in the sensitivity tests based on three influential spectral factors. Top (a, b) for spectral-based wave height to water depth ratio H/h; middle (c, d) for random-sea steepness factor S_p; bottom (e, f) for spectral width parameter ν. Bar graphs show the percentage of the total 16,000 wave buoy data that fall into each range of the sensitivity factor.

errors, which measure the precision, also appear to be lower by up to 13% for the new analytical solution. Fig. 10c and d illustrate the same type of estimates with a very similar result from the deeper measurement stations. Such an agreement between the two physical site conditions can be confirmed by the numbers analyzed in Table 4, all of which appear in the same sign within a comparable range of magnitudes.

In summary, all of the encouraging findings from the above tests may confirm the validities and capabilities of the new analytical formulas. For wave radiation stress, the new solution allows higher accuracy and precision than the traditional representative wave approach, especially in the tests that included wave data from transitional water depths. Such a potential may become obscured under deeper water conditions only because the two different techniques already produce very small estimation errors. The superior performance of the new solution for the wave mass flux M_x appears to be

Table 3
Information of NDBC stations from which spectral wave data were utilized for verifying the new analytical formulas. A total of 7,000 hourly records were obtained from each of the sites.

No.	Site Specification			
	Sta. ID.	Position	h (m)	k_ph [-]
1.	41004	32.501N, 79.099W	38.4	0.90–30.6
2.	41008	31.400N, 80.868W	19.5	0.52–15.5
3.	41009	28.522N, 80.188W	40.5	0.85–32.3
4.	41013	33.436N, 77.743W	23.5	0.68–18.7
5.	42012	30.065N, 87.555W	27.7	0.68–24.1
6.	41025	35.006N, 75.402W	68.3	1.53–49.6
7.	42019	27.907N, 95.352W	82.2	2.84–59.8
8.	42020	26.968N, 96.694W	79.9	2.76–52.7
9.	42036	28.500N, 84.517W	50.6	2.07–36.8

clear in any conditions, provided the solution is applied under the applicable range of $k_ph > \pi/2$.

Among a few attributes, the new solutions are greatest supported by their flexibility to reflect common uncertainties and irregularities in field wave spectra. These proven facts should advocate the use of these new formulas which could readily be executable based on available wind data and physical site conditions. In practice, these closed-form solutions could be incorporated as part of an integrated system for the prediction of wave climatology or in any modeling suites that require such common wave parameters as inputs or modeling variables.

5. Conclusion and discussion

Descriptions of momentum and mass balance over a wave train are important in the study of surface water waves as they allow an explanation for many essential processes in the sea. Wave radiation stress (S_{xx}) and wave mass flux (M_x) are two dynamic parameters that fulfill the descriptions. To determine these parameters, two traditional methods are available, including a numerical means applied on a full wave energy spectrum, and a representative wave approach which relies only on some nominal parameters of the wave field. The advantages of these two options are interchanging between the ability to consider all individual random waves, and the provision of closed-form solutions for analytical applications.

The present research work develops a new set of formulas for the estimation of S_{xx} and M_x while optimizing the preferable capability from each of the traditional options. The problem formulation starts by substituting parameterized wave spectra for an alternative description of the random wave field. The complex non-integrable expressions of both S_{xx} and M_x are first relaxed by use of a simplified wave dispersion relation. Physical asymptotes and calculus of the linear wave theory are then applied as two major keys in the derivation of the new analytical formulas.

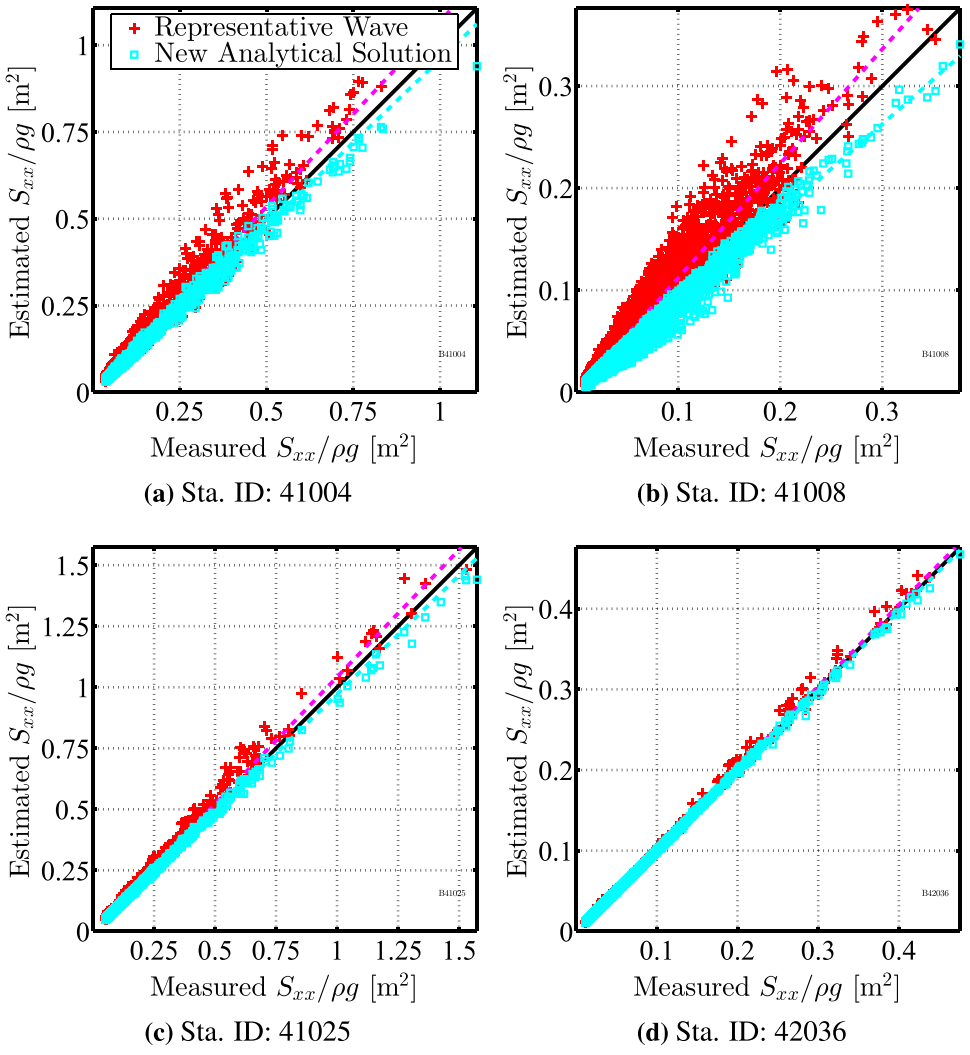

Fig. 9. Comparison between resulting values of wave radiation stress S_{xx} estimated using the two different techniques. Results are shown for two intermediate-deep water sites in (a) and (b), and for two deep water sites in (c) and (d). A summary of the comparison based on all of the data sets may be found in Table 4.

Table 4
Residuals of three statistical indicators found in the comparison of the results from the two different techniques evaluated per nine independent sets of NDBC spectral wave data. Note that negative values indicate superiority of the new formulas, i.e. ΔBIAS for the estimation bias, ΔError for the mean absolute error, and ΔStd. for the standard deviation as percent of the mean.

No.	Sta. ID.	Radiation Stress: S_{xx}			Mass Flux: M_x		
		ΔBIAS [-]	ΔError (%)	ΔStd. (%)	ΔBIAS [-]	ΔError (%)	ΔStd. (%)
1.	41004	−0.03	−1.86	−12.19	−0.10	−9.83	−6.51
2.	41008	0.00	−6.05	−12.60	−0.05	−7.21	−0.12
3.	41009	−0.06	−1.62	−14.71	−0.18	−10.72	−12.97
4.	41013	−0.02	−5.42	−10.75	0.00	−7.01	4.52
5.	42012	−0.01	−0.14	−5.85	−0.20	−10.93	−9.39
6.	41025	−0.02	0.04	−7.21	−0.10	−8.61	−7.42
7.	42019	0.00	0.52	0.10	−0.18	−10.86	−10.87
8.	42020	0.00	0.46	0.28	−0.20	−12.69	−11.40
9.	42036	−0.01	0.97	−2.55	−0.14	−9.04	−12.82

Individual steps in the formulation and the derivation were carefully investigated to reveal that the simplification and asymptotic relationships may lead to non-zero, but apparently insignificant, biases on the resulting parameters. A comprehensive set of synthetic wave data were generated to verify the complete formulas and to find their applicable range over which their estimation performances are greater than those of the representative wave approach. This range is defined on the basis of the proximal water depth factor $k_p h > \pi/2$, for both of the formulas of S_{xx} and M_x.

The new formulas and their sensitivities for various sea states were examined using reliable records of field wave spectra. The relative spectral wave height (H/h) and the sea steepness (S_p) were observed to be important factors, but were, in fact, co-influenced by the relative water depth ($k_p h$). The new solutions appear to work best in lower ranges of H/h and S_p, which are already confined within the applicable limits based on $k_p h$. The most influential sea characteristic seems to be the spreading of wave energy, indicated by the spectral width factor ν. Despite such an influence, for more than 90% of the applicable test cases, the new solutions still provided more accurate estimates than the representative wave approach.

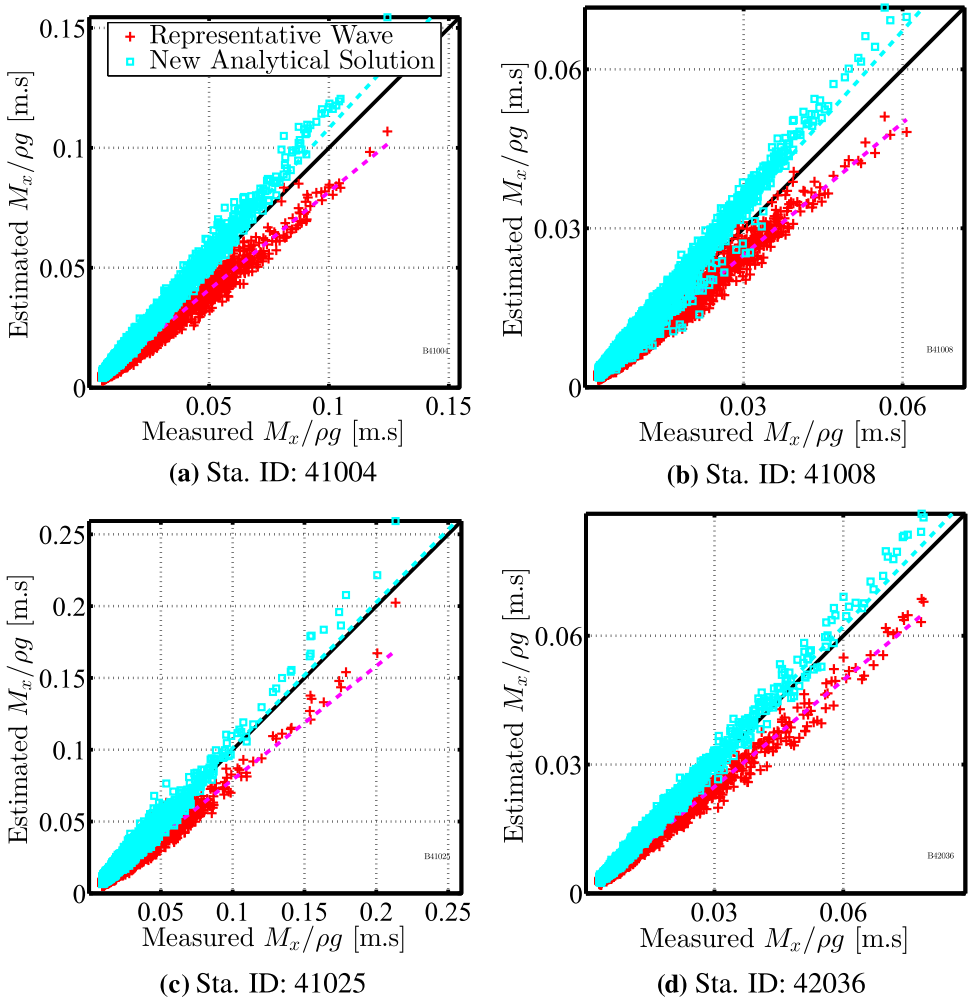

Fig. 10. Comparison between resulting values of wave mass flux M_x estimated using the two different techniques. See Fig. 9 for details.

The new formulas were once again validated against nine independent sets of wave energy spectra obtained by the National Data Buoy Center (NDBC) along the US Atlantic Coast and the Gulf of Mexico. The new formula of S_{xx} was found to allow more accurate and precise estimates than the representative wave approach. This fact is applied in both transitional and deep water conditions, but is especially clear in the former. For the estimation of M_x, performance of the new solution is superior in either condition. Based on the mean errors compared, overall accuracy improvements of around 5% and 10% can be expected for the new formulas of S_{xx} and M_x, respectively. The standard deviations associated with the errors were also up to 15% smaller in the use of the new formulas, which indicate a significant enhancement in the estimation precision.

After all the complex derivation and extensive verification, a simple explanation is possible for the superiority of the new analytical formulas over the traditional approach. While the full numerical method directly accounts for all random waves, the implicit cross-spectrum integration in the new formulas also serves to imitate the process via the use of a parameterized wave spectrum. The actual and the parameterized spectra may not be perfectly matched, but they always share some standard characteristics that are influential for the estimation of the wave parameters, including the spectral shape and the higher and lower bounds of the wave frequencies. The representative wave approach, meanwhile, only accounts for single values of wave height and wave period based on the assumption of a narrow-banded sea. It is this reliance on such ideal conditions that suppresses the capability of the representative wave approach for practical applications on field wave spectra, with much uncertainty and randomness.

In summary, the new analytical formulas introduced in this study are best suitable for the estimation of S_{xx} and M_x of random waves which feature spectral width, steepness, and relative height in the certain ranges of wind-induced waves. The estimation performances are dependent primarily on the local water depth and frequencies of the leading waves. This sensitivity leads to the recommendation that both of the formulas should be applied where the relative water depth factor $k_p h$ appears to be greater than $\pi/2$.

The theoretical development achieved in the present study is expected to be beneficial to the study of surface water waves. The new formulas that appear in closed analytical forms should be easily applied by practitioners in coastal and ocean engineering. The enhancement in the estimation accuracy and precision should encourage the new formulas to be a key upgrade in any modeling tools for wave hydrodynamics and ocean circulation. A research work in progress is aimed at extending the applicability range of the formulas and relaxing their limitation on the wave directionality. An obvious challenge in the further improvement will be on the reformulation of the problem in a very shallow coastal zone where the surface waves and wave-induced velocities do not follow any linear profiles. In such a condition, a nonlinear wave theory may need to be applied, possibly under an intra-wave approach as alternative to the phase-averaged technique.

Acknowledgements

This research project was supported by the Thailand Research Fund (TRF) and Prince of Songkla University, as part of the TRF Grant for New Researcher Program (TRG5880184). The authors are grateful for the kind assistance from all senior scholars and supporting staff at the TRF agency.

References

Bouws, E., Gunther, H., Rosenthal, W., Vincent, C.L., 1985. Similarity of the wind wave spectrum in finite depth water 1. Spectral Form. J. Geophys. Res. Oceans 90 (1), 975–986.
Cambazoglu, M.K., Haas, K.A., 2011. Numerical modeling of breaking waves and cross-shore currents on barred beaches. J. Waterw. Port. Coast. Ocean Eng. 137 (6), 310–323.
Davidson-Arnott, R., 2010. Introduction to Coastal Processes and Geomorphology. Cambridge University Press, UK.
DeVriend, H.J., Stive, M.J.F., 1987. Quasi-3D modelling of nearshore currents. Coast. Eng. 11 (5–6), 565–601.
DeVriend, H.J., Zyserman, J., Nicholson, J., Roelvink, J.A., Pechon, P., Southgate, H.N., 1993. Medium-term 2DH coastal area modelling. Coast. Eng. 21 (1–3), 193–224.
Dean, R.G., Dalrymple, R.A., 1991. Water Wave Mechanics for Engineers and Scientists. Adv. Series on Ocean Eng., Vol. 2. World Scientific, Singapore.
Ding, Y., Wang, S.S.Y., Jia, Y.F., 2006. Development and validation of a quasi-three-dimensional coastal area morphological model. J. Waterw. Port. Coast. Ocean Eng. 132 (6), 462–476.
Eckart, C., 1952. The propagation of gravity waves from deep to shallow water. In: Gravity waves, National Bureau of Standards Circular 521. Vol. 1, pp. 165–173.
Feddersen, F., 2004. Effect of wave directional spread on the radiation stress: comparing theory and observations. Coast. Eng. 51 (5), 473–481.
Haas, K.A., Svendsen, I.A., Haller, M.C., Zhao, Q., 2003. Quasi-three-dimensional modeling of rip current systems. J. Geophys. Res. 108 (C7), 3217–3238.
Haas, K.A., Warner, J.C., 2009. Comparing a quasi-3D to a full 3D nearshore circulation model: SHORECIRC and ROMS. Ocean Modelling 26 (1–2), 91–103.
Hasselman, K., Barnett, T.P., Bouws, E., Carlson, D.E., Hasselmann, P., 1973. Measurements of wind-wave growth and swell decay during the Joint North Sea Wave Project (JONSWAP). Tech. Rep. No. 12, Dt. Hydrogr. Z.
Hoitink, A.J.F., Peters, H.C., Schroevers, M., 2007. Field verification of ADCP surface gravity wave elevation spectra. J. Atmos. Ocean. Technol. 24 (5), 912–922.
Holthuijsen, L.H., 2007. Waves in Oceanic and Coastal Waters. Cambridge University Press, UK.
Hughes, S., 1985. Directional wave spectra using cosine-squared and cosine 2 s spreading functions. Tech. rep., CETN-I-28. Coastal Eng. Res. Center, U.S. Army Engineer Waterways Experiment Station, Vicksburg, MS.
Hughes, S.A., 2004. Estimation of wave run-up on smooth, impermeable slopes using the wave momentum flux parameter. Coast. Eng. 51 (11), 1085–1104.
Li, M., Fernando, P.T., Pan, S., O'Connor, B.A., Chen, D., 2007. Development of a quasi-3D numerical model for sediment transport prediction in the coastal region. J. Hydro-Environ. Res. 1 (2), 143–156.
Longuet-Higgins, M., 1975. On the joint distribution of the periods and amplitudes of sea waves. J. Geophys. Res. 80 (18), 2688–2694.
Longuet-Higgins, M., Stewart, R.W., 1964. Radiation stress in water waves, a physical discussion with applications. Deep Sea Res. 11, 529–563.
Pawlowicz, R., Beardsley, B., Lentz, S., 2002. Classical tidal harmonic analysis including error estimates in MATLAB using T_TIDE. Comput. Geosci. 28 (8), 929–937.
Pierson, W.J., Moskowitz, L., 1964. Proposed spectral form for fully developed wind seas based on similarity theory of S. A. Kitaigorodskii. J. Geophys. Res. 69 (24), 5181–5190.
Rakha, K.A., 1998. A quasi-3D phase-resolving hydrodynamic and sediment transport model. Coast. Eng. 34 (3–4), 277–311.
Soares, C.G., Carvalho, A., 2003. Probability distributions of wave heights and periods in measured combined sea-states from the Portuguese coast. J. Offshore Mech. Arct. Eng. 125 (3), 198–204.
Srisuwan, C., Work, P.A., 2015. Beach profile model with size-selective sediment transport. II: numerical modeling. J. Waterw. Port. Coast. Ocean Eng. 141 (2), 04014033.
Stive, M., Wind, H.G., 1982. A study of radiation stress and set-up in the nearshore region. Coast. Eng. 6 (1), 1–25.
Svendsen, I.A., 2006. Introduction to Nearshore Hydrodynamics. Adv. Series on Ocean Eng. World Scientific, Hackensack, NJ.
Tayfun, M.A., 1986. On narrow-band representation of ocean waves: 1. Theory. J. Geophys. Res.: Oceans 91 (C6), 7743–7752, (1978-2012).
Wang, B., Chadwick, A.J., Otta, A.K., 2008. Derivation and application of new equations for radiation stress and volume flux. Coast. Eng. 55 (4), 302–318.
Wargula, A., Raubenheimer, B., Elgar, S., 2013. The effects of wave forcing on circulation at New River Inlet, NC. Proceedings of Coastal Dynamics 2013, pp. 1871–1880.
Work, P., Srisuwan, C., 2010. Identification of swell in nearshore surface wave energy spectra. Int. J. Ocean Clim. Syst. 1 (2), 51–66.
Work, P.A., 2008. Nearshore directional wave measurements by surface-following buoy and acoustic doppler current profiler. Ocean Eng. 35 (8–9), 727–737.
Young, I., 1994. On the measurement of directional wave spectra. Appl. Ocean Res. 16 (5), 283–294.